Universiteit Antwerpen

Universiteit Antwerpen
Faculteit Wetenschappen
Departement Fysica
Academiejaar 2021-2022

Analog physics with excitations in Bose-Einstein Condensates

Laurent Simons

Dissertation submitted to obtain the degree of
Master Fysica
Proefschrift ingediend ter behaling van de graad
Master Fysica

Supervisors: Prof. dr. Jacques Tempere, Prof. dr. Michiel Wouters

Contents

Acknowledgement

My Master's journey is coming to an end and makes a lot of feelings arise. The best word to describe it would definitely be gratitude. Gratitude for getting the best education I could dream off, gratitude for making me feel part of the team, gratitude for accepting me the way I am, gratitude for everything. Words cannot describe how happy, blessed and privileged I feel to have met all the University of Antwerp Physics professors and to have learned all those amazing things! I am eternally grateful to the University of Antwerp physics department to have taught me all these amazing stuff and for transforming a student with basic high school knowledge about physics into the scientist I have become now equipped with a "toolbox full of knowledge" and ready to enter the arena of the scientific community! Especially, my mentor Prof. Tempere and my co-supervisor Prof. Wouters taught me so much, not only knowledge 'pur sang', but also the know-how to use it ad approach problems in the best way possible; and I am thankful for everything they did for me. They were always there with me during my journey and made me the scientist I am today. I guess now it is up to me to use all those 'tools' they taught me to earn my stripes in the academic world. Also, many thanks to Prof. Carusotto from University of Trento, Italy and Prof. Steinhauer from Technion, Israel for all the interesting talks.

Samenvatting

Bose-Einstein condensaten, die voorspeld werden in 1925 en experimenteel gerealizeerd werden in 1995, bevatten veel interessante phenomenen (zoals superfluiditeit en vortices) [1, 2, 3, 4, 5]. Het is ook een excellente kandidaat voor een kwantum simulator (zoals bedacht door Feynman [6]), om kwantum effecten te simuleren door gebruik te maken van Bose-Einstein condensaten, wat het hoofdonderwerp van deze Thesis is.

In 1974, vermelde Hawking [7] dat zwarte gaten niet compleet zwart zijn, maar ook thermische straling uitzenden. Het grootste probleem is echter dat de temperatuur te laag is om gemeten te worden [8, 9]. Als oplossing, suggereerde Unruh [10] dat een analogie gebruikt kan worden, waar er toegang is tot beide kanten van de horizon, wat het geval is met Bose-Einstein condensaten (met de juiste potentiaal en parameters). Het Casimir effect, waarbij twee ongeladen parallelle platen elkaar aantrekken door vacuum fluctuaties, kan ook gesimuleerd worden met Bose-Einstein condensaten [11, 12, 13, 14, 15]. Beide zijn kwantum effecten die gesimuleerd kunnen worden door Bose-Einstein condensaten.

In deze Thesis, wordt Hawking straling numeriek gesimuleerd door gebruik te maken van een Bose-Einstein condensaat. Een bewegende horizon en een ruimte-afhankelijke interactie sterkte worden gebruikt om de resultaten van [16] te verkrijgen. Ook wordt de experimentele realizatie hiervan besproken.

Twee uitbreidingen worden hieraan nog toegevoegd: (i) een dubbele horizon, een zwarte en een witte, in een de Laval nozzle configuratie waar de kwantum vloeistof eerst versnelt en daarna weer vertraagt, wordt bekeken. (ii) we gingen verder dan de fysica van de uniform bewegende horizon door nog een oscillerende beweging erbij te voegen. Ook werd Bragg spectroscopie gebruikt om de dispersies te meten en gestimuleerde Hawking straling te simuleren door gebruik te maken van een inkomende golf in plaats van kwantum fluctuaties.

De contributie van deze Thesis op dit veld is de gedetaleerde studie van de oscillerende horizon en de de Laval nozzle met een ruimtelijk-gemoduleerde interactie sterkte, terwijl een overzicht over het onderwerp van analoge Hawking straling in BECs wordt uiteengezet.

Het Casimir effect zal worden besproken. Het statische Casimir effect wordt bestudeerd en berekend voor een quasi-1D BEC gebaseerd op [17]. Daarbij, worden schattingen van de Casimir kracht gemaakt voor een experimentele opstelling. Het dynamische Casimir effect zal ook, indirect, behandeld worden in de context van Hawking straling.

Abstract

Bose-Einstein condensates, which were theoretized in 1925 and achieved experimentally in 1995, host lots of interesting phenomena (such as superfluidity and vortices) [1, 2, 3, 4, 5]. It is also an excellent candidate for a quantum simulator (as coined by Feynman [6]), to simulate quantum effects using Bose-Einstein condensates, which will be the main topic of this Thesis.

In 1974, Hawking [7] stated that black holes are not completely black, but emit thermal radiation. The largest problem is, however, that the temperature is too low to be measured [8, 9]. Instead, Unruh [10] suggested that an analogy can be used, where there is access to both sides of the horizon, as is the case with Bose-Einstein condensates (using the right potentials and parameters). Similarly, the Casimir effect, which states that two uncharged parallel plates attract each other due to vacuum fluctuations, can also be simulated using Bose-Einstein condensates [11, 12, 13, 14, 15]. Both are quantum effects which can be simulated by a Bose-Einstein condensate.

In this Thesis, Hawking radiation will be numerically simulated using a Bose-Einstein condensate. A moving horizon and spatially-dependent interaction strength are used to mimic the results of [16]. Additionally, the experimental feasibility of this will be discussed.

Two extensions were added on top of this model: (i) a double horizon, one black and one white, in a de Laval nozzle configuration where the quantum fluid is first accelerated and subsequently decelerated, was considered. (ii) we went beyond the physics of the uniformly moving horizon by adding an oscillatory motion on top of the linear motion. Also Bragg spectroscopy was used to measure the dispersions and simulate stimulated Hawking radiation by using, an incoming wave instead of quantum fluctuations.

The contribution of this Thesis to this field is the detailed study of the oscillating horizon and the de Laval nozzle with a spatially-modulated interaction strength, while reviewing the topic of analog Hawking radiation in BECs.

The Casimir effect will be discussed. The static Casimir effect will be studied and calculated for a quasi-1D BEC based on [17]. In addition, estimates of the Casimir force will be made for an experimental setup. The dynamical Casimir effect will, indirectly, be covered in the context of Hawking radiation.

List of Figures

List of Tables

Chapter 1

Introduction

1.1 Introduction and state of the art

In 1974, Hawking [7] theorized that black holes are not completely black. Hawking used quantum field theory, in combination with general relativity to predict that black holes emit radiation according to a Planck spectrum with a certain temperature. This radiation is a result of the vacuum fluctuations at the event horizon which produce pairs of particles, where one of the particles gets attracted to the singularity. The other particle will be measured as radiation. After theoretical calculations of the expected temperature, a major problem was faced: the temperature for astrophysical black holes is so low that the radiation is too weak to be measured over the cosmic microwave background [8, 9].

However, in 1976, Unruh [10] suggested to model gravitational fields from general relativity using other physical systems, such as a fluid. Working with such analogies has become known as "analog gravity", and it can be extended to "analog physics" for other phenomena such as the Casimir effect. This is the foundation of this thesis, where we investigate the use of Bose-Einstein condensates to simulate event horizons, Hawking radiation, and the Casimir effect.

In a Bose-Einstein condensate, using an analogy between the speed of sound (the phononic excitations) and the speed of light, an artificial horizon can be created by using a potential step [8, 9]. A cartoon illustration of the sonic black hole is shown in Figure 1.1. However, even in a Bose-Einstein condensate, the temperature is too weak to be detected [8, 9]. Fortunately, in this case, there is access to both sides of the horizon [8, 9]. Now, correlations between the Hawking pairs at both sides of the horizon can be measured [8, 9]. Several papers about this have already been published and here only an overview of the state of the art is given.

In 2008, Carusotto *et al.* [16] already made extensive simulations of this system by using a step potential which moves through the condensate with a certain speed, which needs to be in between the speed of sound of both sides of

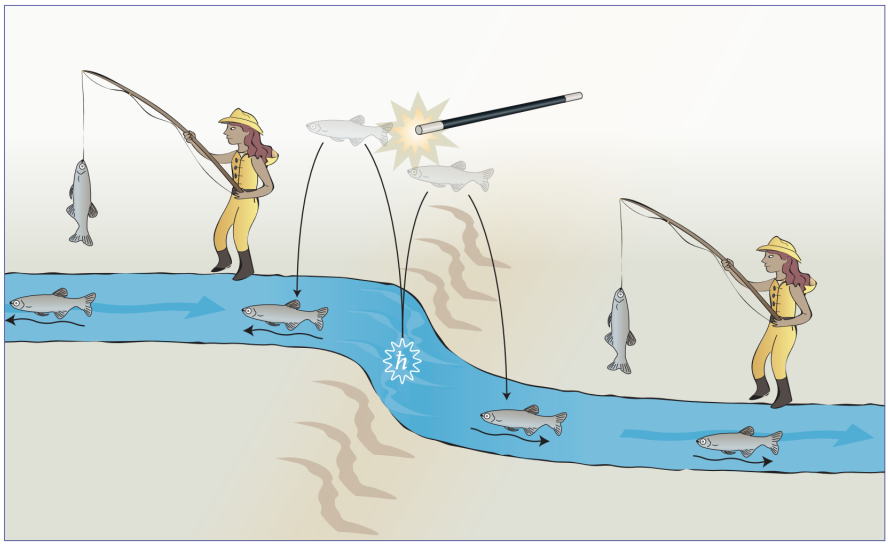

Figure 1.1: In this cartoon picture, the waterfall which accelerates the flow is the horizon [18]. From vacuum fluctuations, pairs of fish are created at the waterfall, headed in opposite directions. Note that the flow velocity at the waterfall is larger than the swimming speed of the fish, so the downstream fish can never reach the upstream region any more, even if it reversed course. Both fish can be caught by fishers at opposite sides of the waterfall and this illustrates the correlation between the fish at both sides (Hawking radiation) [18]. Source: [18].

the horizon [16]. They used a spatially-varying interaction strength to minimize deterministic effects such as soliton-shedding and the production of shock waves at the barrier [16]. Their simulation revealed two Hawking modes, and a pair of fringes related to the dynamical Casimir effect [16]. The latter is due to the spatially-varying interaction strength [16]. Following this, experimental studies have been performed. One of the most prominent ones are from Steinhauer. In 2014, he studied stimulated Hawking radiation, which makes use of two horizons (inner and black hole horizons) to amplify the Hawking radiation (just as in a laser) [19]. This would give rise to a checkerboard pattern. This was numerically simulated by Wang [20]. In 2015 and 2016, spontaneous Hawking radiation was observed experimentally and the entanglement between the particles at both sides of the horizon was studied [21, 22]. And in 2019, the thermality of Hawking radiation was tested [23]. Also, several theoretical studies have been performed. In this thesis, the result of Carusotto, [16], will be reproduced and the experimental feasibility is studied. We go beyond the proposal by Carusotto et al. by studying a double horizon configuration where the radiation created by one horizon can be 'amplified', and by considering an oscillating motion of the horizon.

A closely related effect, which has its origins in quantum fluctuations of the vacuum too, is the Casimir effect. The Casimir effect states that two uncharged parallel plates attract each other due to the modification of the vacuum fluctuations between them [12, 13, 14, 15]. So, this is a quantum effect. Now, a similar analogy can be applied here: Bose-Einstein condensates and their excitations can be used to study the Casimir effect.

In addition to the static Casimir effect leading to the force on parallel plates, there is a dynamical Casimir effect that arises when a system parameter is suddenly changed and the virtual particle vacuum fluctuations turn real. Their correlation properties are similar to those emitted by Hawking radiation as will be in this thesis.

There have already been several theoretical studies [24, 17] as well as experimental studies [25, 26] of the dynamical Casimir effect. Also, studies have looked at the measurement of the Casimir-Polder force [27]. Ref. [17] describes the derivation of the Casimir force in the case of a quasi-1D condensate trapped between two plates, which will be used later on in this thesis. Refs. [25, 26] describe the measurement of the dynamical Casimir effect by using a spatially-varying interaction strength which can take on many forms. A step potential form is used in [16] which will be discussed in this thesis as well. The experimental feasibility of the measurement of the static Casimir effect is studied for the RuBECi setup, designed by ColdQuanta, which will be used in the University of Antwerp and Ghent for experiments on Bose-Einstein condensates.

1.2 Thesis outline

The overal goal of this Thesis is to get an overview of analog gravity and the analog Casimir effect in Bose-Einstein condensates. For the former, different

setups were considered. First, the moving step experiment is simulated, as was previous done in [16]. The de Laval nozzle and the oscillating horizon experiment were analyzed too. Lastly, a short section was dedicated to Bragg spectroscopy and how it is used to stimulate Hawking radiation. This thesis is structured as follows:

- **Chapter 2: Theoretical Background** - In this chapter, the necessary theoretical background will be given. This includes: a short recap about Bose-Einstein condensates (what they are, the theory describing them and the excitations that play a role), the Casimir effect in electromagnetism and Hawking radiation. Also, a short introduction will be given into the field of analog physics.

- **Chapter 3: Numerical techniques** - Chapter 3 describes the different numerical techniques which are needed in this thesis. First of all, the pseudo-spectral split-step method used to solve the Gross-Pitaevskii equation will be explained. Secondly, the Truncated Wigner approximation will be shown, which is used for the incorporation of quantum fluctuations in our simulations.

- **Chapter 4: Hawking radiation and other excitations** - The analogy between Hawking radiation in black holes and Bose-Einstein condensates will be explained and the step-sweep experiment of [16] will be studied. Also, the experimental feasibility will be reasoned. The oscillating horizon experiment will be introduced and several other effects will be discussed. The Laval nozzle is studied, as well. Furthermore, Bragg spectroscopy will be shown and the relation with stimulated Hawking radiation will be considered.

- **Chapter 5: Static Casimir effect** - Here, the derivation of the static Casimir effect for a quasi-1D Bose-Einstein condensate will be studied [17] and the RuBECi setup will be discussed. Lastly, the experimental feasibility will be discussed.

- **Chapter 6: Conclusion and Outlook** - In this chapter, the conclusion will be given and possibilities for further studies will be touched on.

Chapter 2

Theoretical Background

In this chapter, the necessary theoretical background is given. First, Bose-Einstein condensates and the Casimir effect in the context of electromagnetism will be studied. Secondly, Hawking radiation in general relativity will be introduced. Also, the field of analog physics and its applications are shown.

2.1 Bose-Einstein condensates

Although Bose-Einstein condensation was already predicted in 1924 by Einstein [28], it took till 1995 to be realized by Cornell, Wieman, Ketterle, and Hulet [2, 3, 29]. The properties that a cooled gas of bosons manifest are of interest to researchers as an controllable quantum many-particle system for the study of weakly interacting superfluids, that are theoretically much easier to deal with than with the strongly interacting helium superfluid. Their fermionic counterparts are actively used as simulators for superconductors. Beyond these relatively obvious analogs, they can also be used as a gateway to study other experimentally out-of-reachable systems, like black holes. The search for Bose-Einstein condensation sparked interest in finding different cooling methods. Since the proposal of this new state of matter, several theories were proposed to describe it, including the Gross-Pitaevskii equation [30, 31]. Following the discovery of Bose-Einstein condensates, other systems, including the Fermionic condensate, were proposed and discovered [32]. All of these topics will be shortly discussed here. The book of Pitaevskii and Stringari [33] and the course notes of Prof. Tempere [1] are used as a thread through this section and can be consulted by the interested reader.

2.1.1 Introduction

Boltzmann's classical description of atoms (e.g, kinetic theory of gases) in a gas describes atoms as mass points that possess a particular position and momentum and collide with each other. When the gas cools down, the atoms have less

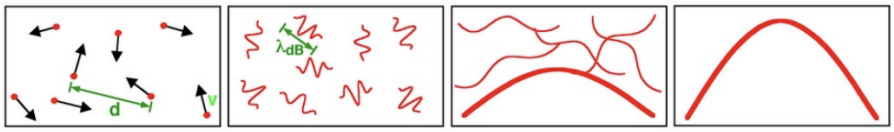

Figure 2.1: While decreasing the temperature, the wavelength becomes larger and larger and at some point, they interfere constructively to form one collective "quantum wave". Source: [38].

momentum and thus move slower. The mean kinetic energy of a gas of atoms is given, classically, by [34]:

$$E_{\text{kin}} = \frac{\langle p^2 \rangle}{2m} = \frac{3}{2} k_B T, \tag{2.1}$$

where m represents the mass of the atoms, k_B is Boltzmann's constant, and T is the temperature. In 1923/1924, Louis de Broglie [35, 36] introduced the idea that all particles should be seen as wavepackets which correspond with a spread on position and momentum, which are related to each other by Heisenberg's uncertainty principle $\Delta x \Delta p \geq \hbar/2$ with $\hbar$ Planck's constant. The spread on the position can be related to the temperature via the de Broglie wavelength [4]:

$$\lambda_{\text{dB}} = \sqrt{\frac{2\pi\hbar^2}{m k_B T}}. \tag{2.2}$$

This can be interpreted as follows: when cooling the gas down, the momentum decreases and thus also the uncertainty on the momentum ($\Delta p < \sqrt{\langle p^2 \rangle}$), and through the Heisenberg's uncertainty principle, the spread on position increases. The ratio between the spread of the wave packet and the distance between the particles can be described by the phase space density $n\lambda_{\text{dB}}^3$. For air at room temperature, the phase space density is approximately 10^{-7}. When the gas cools down a significant amount (so, when $n\lambda_{\text{dB}}^3 = 1$), the wavefunctions of the atoms can overlap. Here the case of bosons, which are particles with integer spin which obey Bose-Einstein statistics, will be discussed because, with fermions, multiple particles cannot take on the same wavefunction [37]. The bosons will then tend to macroscopically occupy the single-particle ground state, and the wavefunctions interfere constructively, resulting in one collective "quantum wave". This is called a *Bose-Einstein Condensate* (BEC) and is schematically shown in Figure 2.1. The BEC phenomenon was already predicted by Bose and Einstein in 1924 [28], however, it took till 1995 to observe a BEC (due to the, back then unavailable, cooling techniques) [2, 3]. Bose-Einstein condensation was discovered by Cornell, Wieman for rubidium atoms, and by Ketterle for sodium atoms in 1995. They received the Nobel prize for their work in 2001.

2.1.2 Experimental technologies

The main impediment for achieving Bose-Einstein condensates of dilute gases was the low temperature needed, which is of the order of μK. Several cooling methods were invented and a few of them are discussed. This discussion is based on [1, 39]. One of the first attempts (apart from using liquid nitrogen, which cools till around 70 K) was made by Heike Kamerlingh Onnes, who used liquid helium to cool systems. He reached temperatures of a few Kelvins. However, this was still not sufficient, so other, more sophisticated methods were needed. The different methods used for cooling include:

1. Laser cooling (or Doppler cooling): using laser light to slow down the atoms [40, 41, 42]
2. Evaporative cooling: the most energetic atoms are pulled out of the trap
3. Simultaneous and sympathetic cooling [43]

Laser cooling

In vacuum, when cooling a dilute gas down it does not become a liquid or solid, but it stays a gas of atoms [44]. So, decreasing the temperature is associated with slowing down the atoms [44]. There are already multiple techniques to slow down electrically charged particles, such as the usage of electric and magnetic fields [44]. However, a method to cool down electrically neutral atoms (in general) is requested. Laser cooling is a type of cooling discovered by Cohen-Tannoudji, Chu, and Phillips and proposed by Hänsch and Schawlow in 1975 [40, 41, 42], where the laser beam slows down most of the atoms. This works also for electrically neutral atoms [44]. The principle is schematically represented in Figure 2.2. A photon from the laser beam with momentum $\hbar k$ frontally collides with an atom of the gas, which possesses a velocity v and gets absorbed. This results in a decrease in the atom's speed $v - \hbar k/m$. After spontaneously re-emission of the -now- redshifted photon, the atom stays slow. This also slows down the atoms because a redshifted photon has lower energy than the original absorbed photon. This will lead to temperatures of the order of tens of microkelvins.

Magneto-Optical Traps (MOTs)

Atoms can be magnetically trapped by making use of magnetic fields. This can be accomplished by using laser cooling as illustrated in Figure 2.3. The atoms will favorably absorb the photons, which push them back, so confining the atoms. Trapping can be improved by noting that the resonant frequency of the hyperfine transition will be influenced by the Zeeman splitting of the levels in a magnetic field (which can be created by using Helmholtz coils). Three laser beams in three different directions and adding a magnetic field (could be spatially varying) results in a Magneto-Optical Trap (MOT).

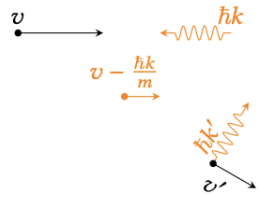

Figure 2.2: Laser cooling. (a) the photon from the laser and the atom collide which through absorption results in (b) a slowed down atom which (c) spontaneously re-emits the photon (which is then redshifted), while the atom still stays slow. Source: [39].

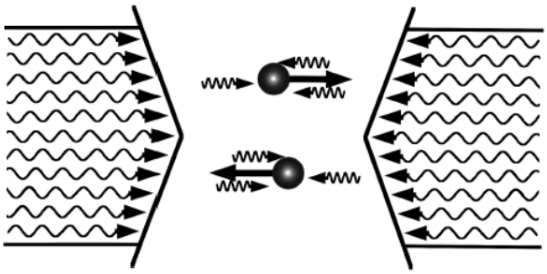

Figure 2.3: The principle behind (a one-dimensional) MOT: Laser cooling using two laser beams. The atoms will preferentially absorb the photons which push them back. Source: [1].

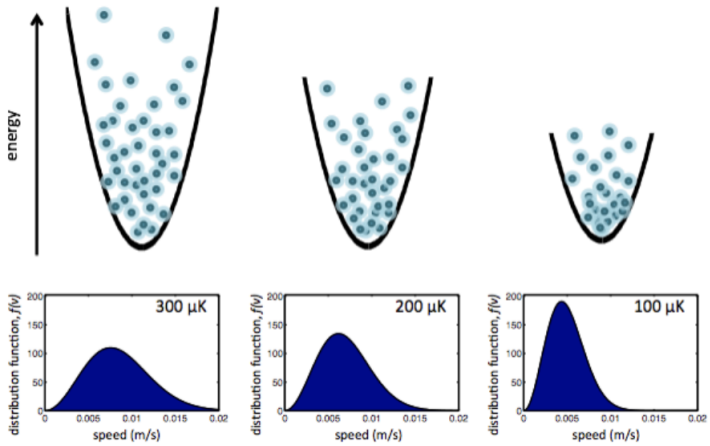

Figure 2.4: Illustration of evaporative cooling. The atoms with the most energy will reach the top of the well and escape. The velocity distribution is also shown. Source: [45].

Evaporative cooling

The temperature obtained by laser cooling is not enough to achieve Bose-Einstein condensation. Therefore, the last step is to perform evaporative cooling. Here a radiofrequent electromagnetic field is used to induce a change of spin in the atoms, which alters the magnetic moment such that these atoms are removed from the condensate. By making the radiofrequent field only resonant in certain regions, it is possible to select which atoms (e.g., most energetic ones) are removed. Now, the atoms in the remaining cloud have smaller average energy which corresponds to a lower temperature. The general idea is illustrated in Figure 2.4. This cooling technique allows to reach nanokelvin temperatures.

2.1.3 Theoretical description

The Bose-Einstein condensate can be described by using a complex-valued order parameter Ψ, which is proportional to the single-particle wave function ϕ_0 that all the particles occupy: $\Psi = \sqrt{N_0}\phi_0$, where N_0 is the number of particles in the condensate. The modulus squared of the order parameter can be interpreted as the density of condensed particles, and the phase gradients of the order parameter are proportional to the velocity field for the condensate. This order parameter satisfies a nonlinear extension of the Schrödinger equation, the so-called *Gross-Pitaevskii equation* [30, 31]:

$$i\hbar\frac{\partial}{\partial t}\boldsymbol{\Psi}(\boldsymbol{r},t) = -\frac{\hbar^2}{2m}\nabla^2\boldsymbol{\Psi}(\boldsymbol{r},t) + V_1(\boldsymbol{r},t)\boldsymbol{\Psi}(\boldsymbol{r},t) + \frac{4\pi\hbar^2 a}{m}|\boldsymbol{\Psi}(\boldsymbol{r},t)|^2\boldsymbol{\Psi}(\boldsymbol{r},t). \quad (2.3)$$

Here $V_1(\mathbf{r})$ stands for an external potential (which frequently is a harmonic trap) and a stands for the s-wave scattering length. The latter depends on the type

of atoms that are considered that interact and of the hyperfine state of the two interacting atoms. A list of the s-wave scattering length is given for different atoms in Table 2.1. Here the interatomic potentials have been approximated by a contact potential:

$$V_2(\mathbf{r}-\mathbf{r'}) = \frac{4\pi\hbar^2 a}{m}\delta(\mathbf{r}-\mathbf{r'}). \tag{2.4}$$

$4\pi\hbar^2 a/m$ is frequently denoted by g, which is called the interaction strength. This interaction strength could be constant. However, it could become spatially-dependent. There are multiple ways to change g. One is by using the Feshbach resonance [46, 47]. There the interaction strength g can be varied by changing the magnetic field applied B. The main idea behind it is, that when the energy of a bound molecular-like state of the two scattering atoms, which is influenced by an external magnetic field, is equal to the energy of the scattering atoms in an open scattering channel, a resonance effect occurs which in turn results in an enhanced scattering length a_s [47, 46]. Early works in regard to the Feshbach resonance have been performed by [48] and [49]. A review of the Feshbach resonance effect in ultracold gases is given in [46] (for the interested reader). The dependence of the scattering length on the magnetic field with the Feshbach resonance around B_0 with width ΔB is [46]:

$$a(B) = a_{\mathrm{bg}}\left(1 - \frac{\Delta B}{B - B_0}\right), \tag{2.5}$$

where a_{bg} represents the "background" scattering length far away from the resonance. This is depicted in Figure 2.5.

A second way of changing g is, in the case of a 1D or 2D condensate, by changing the confinement. So, a 1D (2D) condensate is obtained by having strong confinement in two (one) directions such that $gn \ll \hbar\omega_{\mathrm{direction}}$. The so-called 'effective' interaction strength in 1D is: $g_{1D} \sim g_{3D}/\ell^2$ (as will be discussed in more detail in Chapter 5). By changing the confinement frequency, ℓ changes and thus g_{1D} changes. It could, for example, be made x-dependent by having a confinement frequency in the y and z direction which depends on x. This will be used later on.

Note that the Gross-Pitaevskii energy functional describes a gas of bosons which are *weakly* interacting, i.e. $na^3 \ll 1$. Values of the background scattering length for several widely used atom species are given in Table 2.1. From the Gross-Pitaevskii equations, two other useful equations can be derived. First, multiply the time-dependent GP equation by $\Psi^*(r,t)$ and subtract its complex conjugate:

$$\frac{\partial|\Psi(\boldsymbol{r},t)|^2}{\partial t} + \nabla\cdot\left(\frac{\hbar}{2mi}(\Psi^*(\boldsymbol{r},t)\nabla\Psi(\boldsymbol{r},t) - \Psi(\boldsymbol{r},t)\nabla\Psi^*(\boldsymbol{r},t))\right) = 0. \tag{2.6}$$

Rewriting results in a continuity equation:

$$\frac{\partial n}{\partial t} + \nabla\cdot(n\boldsymbol{v}) = 0, \tag{2.7}$$

Atomic species	a in units of a_{Bohr}
^{7}Li	-27.6
^{23}Na	65.3
^{41}K	65
^{87}Rb	106

Table 2.1: The s-wave scattering length for different atomic species in units of the Bohr radius. Note that for some atoms it is attractive and for some it is repulsive. Source: [1]

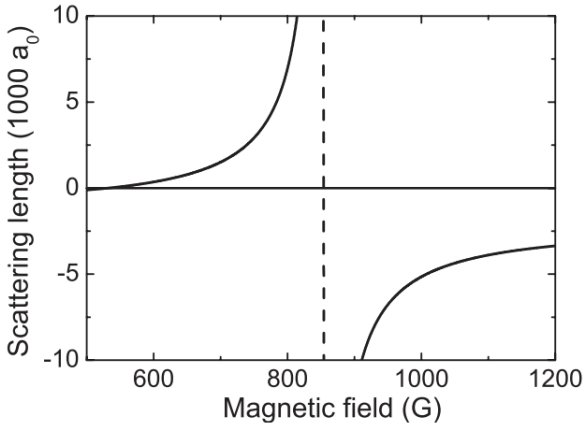

Figure 2.5: The Feshbach resonance displays the dependence of the scattering length on the magnetic field, in the case of lithium atoms [47]. The scattering length is normalized to a "background" scattering length. The scattering length can thus be varied over a large range (here, over an order of magnitude) [47]. Source: [50].

with a velocity field:

$$\boldsymbol{v} = \frac{\hbar}{2mi}\frac{\Psi^*\nabla\Psi - \Psi\nabla\Psi^*}{|\Psi|^2}. \tag{2.8}$$

The wavefunction can be represented by $\Psi = \sqrt{n}e^{iS}$. This results in:

$$\boldsymbol{v} = \frac{\hbar}{m}\nabla S \text{ and } \nabla \times \boldsymbol{v} = 0. \tag{2.9}$$

Now, for the second equation, plug in the phase representation of the wavefunction in to the GP equation and seperate the real components:

$$\hbar\frac{\partial S}{\partial t} + \left(\frac{\hbar^2}{2m}(\nabla S)^2 + V_1 + \frac{4\pi\hbar^2 a}{m}n - \frac{\hbar^2}{2m\sqrt{n}}\nabla^2\sqrt{n}\right) = 0. \tag{2.10}$$

This is the second equation, next to the continuity equation. These equations will be referred to as the hydrodynamic equations later on. Note that the second

equation is Euler's equation for a frictionless and non-viscous fluid. That is a manifestion of the superfluid nature of atomic Bose-Einstein condensates.

In order to understand the characteristic length scale of the Gross-Pitaevskii equation, the one-dimensional problem with a hard wall at $x = 0$ is studied. The Gross-Pitaevskii equation in one dimension with the boundary conditions $\Psi(0) = 0$ en $\Psi(\infty) = \sqrt{n_\infty}$, has a solution for $x > 0$, which is given by [33]:

$$\Psi(x) = \sqrt{n_\infty} \tanh\left(\frac{x}{\xi\sqrt{2}}\right). \tag{2.11}$$

The characteristic length scale over which the order parameter can vary is ξ , the "healing length". This is the length scale where the kinetic energy equals the interaction energy, and it is given by [33]:

$$\xi = \frac{1}{\sqrt{8\pi a n}}. \tag{2.12}$$

Typically, the healing length is of the order of 100 nm up to a micron in experimental realizations of atomic Bose-Einstein condensates. The previous solution was obtained from solving the time-independent Gross-Pitaevskii equation (which can be deduced from the time-dependent equation by using a time-dependency of the solution of the form $e^{-i\mu t/\hbar}$) in one dimension and in the case of a hard wall at $x = 0$. Far from the wall, the 'bulk' solution of a uniform condensate is retrieved [33]:

$$\mu = \frac{4\pi\hbar^2 a}{m} n_\infty = g n_\infty. \tag{2.13}$$

This expression is not completely valid anymore in a 1D situation, as the relation between g and the 3D scattering length a becomes more complicated. Nevertheless, μ remains equal to gn_∞. The chemical potential can be interpreted as the work that is necessary to remove a particle. It is an important energy scale for the Bose-Einstein condensate.

2.1.4 Excitations

This section is based on [51, 33]. Consider a stationary solution $\Psi_0(\mathbf{r})$ of the Gross-Pitaevskii equation and add a small perturbation:

$$\Psi(\mathbf{r}) = e^{-i\mu t/\hbar}(\Psi_0(\mathbf{r}) + \delta\psi(\mathbf{r}, t)). \tag{2.14}$$

The Gross-Pitaevskii equation becomes (retaining only the terms linear in $\delta\psi$ and $\delta\psi^*$):

$$i\hbar\frac{\partial}{\partial t}\delta\psi = \left[-\frac{\hbar^2}{2M}\nabla^2 + V_{ext} - \mu\right]\delta\psi + g|\Psi_0|^2\delta\psi + g\Psi_0^2\delta\psi^*, \tag{2.15}$$

$$i\hbar\frac{\partial}{\partial t}\begin{pmatrix}\delta\psi \\ \delta\psi^*\end{pmatrix} = \begin{bmatrix} H_{GP} + g|\Psi_0|^2 - \mu & g\Psi_0^2 \\ -g\Psi_0^{*2} & -(H_{GP} + g|\Psi_0|^2 - \mu)\end{bmatrix}\begin{pmatrix}\delta\psi \\ \delta\psi^*\end{pmatrix}. \tag{2.16}$$

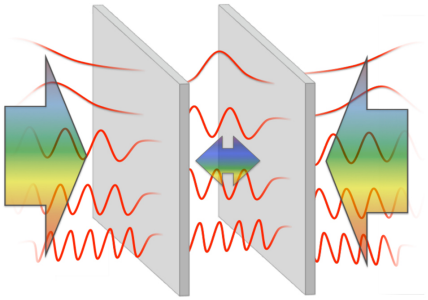

Figure 2.6: An illustration of the setup used to explain the Casimir effect in electromagnetism. Source: [55].

This is called the time-dependent Bogoliubov-de Gennes equation. In the case of an homogeneous condensate, it simplifies to:

$$i\hbar\frac{\partial}{\partial t}\begin{pmatrix}\delta\psi\\ \delta\psi^*\end{pmatrix}=\begin{bmatrix}\frac{\hbar^2k^2}{2m}+gn & gn\\ -gn & -(\frac{\hbar^2k^2}{2m}+gn)\end{bmatrix}\begin{pmatrix}\delta\psi\\ \delta\psi^*\end{pmatrix}, \tag{2.17}$$

with eigenvalues:

$$\hbar\omega_k=\pm\sqrt{\frac{\hbar^2k^2}{2m}\left(\frac{\hbar^2k^2}{2m}+2gn\right)}. \tag{2.18}$$

This represents the Bogoliubov dispersion relation. In the long-wavelength limit or for small momenta, the frequency is linear in the momentum with a proportionality factor, called the *speed of sound*:

$$c_s=\sqrt{\frac{gn}{m}}. \tag{2.19}$$

This will be an important quantity when considering Hawking radiation in condensates; the gravitational analogy for the speed of sound (2.19) is the speed of light.

2.2 Casimir effect

In electromagnetism, the *Casimir effect* refers to the attraction of two uncharged parallel perfectly conducting plates which are located at a small distance d with respect to each other in a vacuum, where quantum vacuum fluctuations, which lie at the basis of this effect, produce "macroscopic" effects [11, 12, 13, 14, 15]. It was first predicted by Casimir [52, 53] and later experimentally verified by Lamoreaux [54] with great accuracy.

Consider two neutrally charged plates with equal area A which are separated with a distance d. This is illustrated in Figure 2.6. The zero-point energy of

the vacuum gives rise to a force given by:

$$F = -\frac{\hbar\pi^2 cA}{240d^2}. \tag{2.20}$$

It is negative because it is an attractive force and of course it is proportional to the area of the plates. Now, the force is very small and therefore hard to be observed, experimentally. First of all, instead of a plate a part of a large sphere is used, because it is hard to make two plates parallel on a small distance [56]. Furthermore, there are a lot of corrections which need to be taken into account (such as temperature) [56]. These will not be discussed here. Finally, atomic force microscopy (AFM) is used [56]. There, the large sphere is attached to a 'rod' which moves because of the plate. Due to recent developments, these changes are measurable.

The Casimir effect is also used in many other fields in physics, such as quantum field theory and condensed matter physics [57]. In general, the Casimir effect can be defined as the created force, where bosons result in an attractive contribution and fermions in a repulsive contribution when a quantum field is enclosed in a finite space volume [57, 58]. The dynamical Casimir effect is similar to the (static) Casimir effect, however, a quick change of boundary conditions is applied that results in the creation of real particles [26].

To explain it informally, the static Casimir effect is a result of vacuum fluctuations which result in creation and annihilation of pairs of virtual particles [59]. Outside of the plates, the virtual photons may have any wavelength [59]. However, inside the plates the possible wavelengths are restricted [59]. The outside virtual photons create a force against the plates [59]. However, the inside virtual photons create an opposite 'smaller' force [59]. There will be a net attractive force between the plates [59].

A Bose-Einstein condensate can also be used where there is still a Casimir force present which can be measured as long as it is confined between two plates [24]. An example is a BEC confined in a cylindrical tube, like in [60]. The Casimir effect studied till now is called the *static* Casimir effect, where the position or geometry of the boundaries remain unchanged. In the chapter 5 of this thesis, we will explore the static Casimir effect in more detail.

The *dynamical* Casimir effect is associated with the production of quasi-particles due to a sudden change in boundary conditions, such as geometry and position of the boundaries [26]. Such a sudden change in boundary conditions can be realized by moving mirrors [26, 24, 60]. It can be realized by changing the index of refraction as well [26, 24, 60]. Another possibility is the change of the scattering length, as an obvious consequence of the change in the speed of sound/light, due to the use of the Feshbach resonance [26, 47]. Here, the Casimir effect is caused by phononic excitations [61].

2.3 Hawking radiation

2.3.1 Black holes

This section is based on [62] and serves as an introduction to black holes and general relativity for the reader. In general relativity, gravity is not a force but is a phenomenon that arises because of the curvature of spacetime or like physicist J. Wheeler puts it: "*Spacetime tells matter how to move; matter tells spacetime how to curve.*". The geometry of spacetime can be described by the *metric tensor* $g_{\mu\nu}$ which can be related to an infinitesimal line element by:

$$ds^2 = g_{\mu\nu} dx^\mu dx^\nu. \tag{2.21}$$

The *Christoffel symbols* are defined as:

$$\Gamma^\sigma_{\mu\nu} = \frac{1}{2} g^{\sigma\rho}(\partial_\mu g_{\nu\rho} + \partial_\nu g_{\rho\mu} - \partial_\rho g_{\mu\nu}), \tag{2.22}$$

and the *Riemann tensor* is defined as:

$$R^\rho_{\sigma\mu\nu} = \partial_\mu \Gamma^\rho_{\nu\sigma} - \partial_\nu \Gamma^\rho_{\mu\sigma} + \Gamma^\rho_{\mu\lambda}\Gamma^\lambda_{\nu\sigma} - \Gamma^\rho_{\nu\lambda}\Gamma^\lambda_{\mu\sigma}, \tag{2.23}$$

where Einstein's summation convention is used. The space is flat when every component of the Riemann tensor is zero. *Einstein's equation* is a generalization of the Poisson equation for the Newtonian potential:

$$\nabla^2 \Phi = 4\pi G\rho, \tag{2.24}$$

and tells us how the metric (and thus curvature) is related to the presence of energy and momentum. It is given by:

$$R_{\mu\nu} - \frac{1}{2} R g_{\mu\nu} = 8\pi G T_{\mu\nu}, \tag{2.25}$$

where $R_{\mu\nu} = R^\sigma_{\mu\sigma\nu}$ is the Ricci tensor, $R = R^\mu_\mu$ is the curvature scalar and $T_{\mu\nu}$ is the energy and momentum tensor. A spherically symmetric vacuum ($T_{\mu\nu} = 0$) solution to this equation is the *Schwarzschild solution*:

$$ds^2 = -\left(1 - \frac{2GM}{r}\right) dt^2 + \left(1 - \frac{2GM}{r}\right)^{-1} dr^2 + r^2 d\theta^2 + r^2 \sin^2\theta d\phi^2. \tag{2.26}$$

It has two points (singularities) where a component of the metric tensor diverges: $r = 0$ and $r = 2GM$. To check if these are really singularities, every component of the Riemann tensor should be checked to see if the curvature is infinite. However, the notion of a tensor component being infinite is ambiguous because a tensor is not invariant under a coordinate transformation. So, scalars, that can be constructed from the Riemann tensor, should be checked. The spacetime has one singularity at $r = 0$ and the other point $r = 2GM$ is the Schwarzschild radius and is a coordinate singularity; the coordinates which were chosen were poor. Nevertheless, it is still an interesting point. When particles enter the event horizon, there is no way back. An object which has an event horizon that separates it from the rest of space is called a *black hole*.

2.3.2 Hawking and Unruh radiation

This section is mainly based on [62][1]. A uniformly accelerating, with magnitude a, observer (called a Rindler observer) will observe the vacuum as a thermal bath of temperature $T = \frac{\hbar a}{2\pi ck}$ [63, 64, 65, 66]. This effect is called the *Unruh effect* [10], where a flat space-time (Minkowski space) is assumed.

Hawking radiation is the thermal bath that an observer outside the black hole perceives and has a temperature $T = \frac{\hbar g}{2\pi ck}$ with g the local acceleration due to gravity [63, 64]. This is related to Unruh radiation in the sense that an accelerated observer in the absence of gravity is equivalent (locally) to an observer in rest in the presence of gravity [2][63].

Classically a black hole is "black". But, quantum-mechanically it is not black and it is a black body with a temperature of $T = \frac{\hbar g}{2\pi ck}$.

It is intricate to observe and measure Hawking-Unruh radiation because to produce a temperature of one microkelvin, an acceleration of the order of 10^{14} m s^{-2} is required. Ultra-cold atoms can help [67]. As suggested by Unruh [10], Hawking radiation is a kinematic effect of QFT [68]. So, any system can be used to study Hawking radiation as long as it has a similar analog curved spacetime (see next section). In our case, Bose-Einstein condensates have a similar hydrodynamic effective metric [9]. Note: in this case, the thermality of the Hawking radiation is still small, however here, access to both sides of the horizon is possible [9]. Therefore, correlations between both sides can be studied [9]. The connection with the dynamical Casimir effect can be directly observed. In the case of the dynamical Casimir effect, real particles/photons are created by an accelerating plate [59]. With black holes, real particles are created, similarly to the dynamical Casimir effect where gravity plays the role of acceleration (see the weak equivalence principle) [59].

2.4 Analog physics

As mentioned earlier, astrophysical Hawking radiation is characterized by a temperature which is small and thus challenging to measure [8]. Fortunately, Bill Unruh [10] introduced the notion of *analog spacetimes* which are able to simulate the kinematic part of General Relativity (GR) [8, 9]. However, they are not able to simulate the dynamic part relating to the Einstein equations [8]. This is enough to describe the Hawking radiation effect,however not, for instance, Bekenstein entropy which is related to the dynamical part of GR [8]. Analog spacetimes work with effective metrics which can be established by splitting the system in two parts: the background and a perturbation [8]. There are several analog systems which can be utilized [8]. For example, the surface waves on water or optical pulses in mediums [8]. The one which will be of interest to us are bulk acoustics in a fluid [8]. In general, analog models are

[1] Be aware of the used units with $c = 1$

[2] Refer to the Weak Equivalence Principle (WEP): "The motion of freely-falling particles are the same in a gravitational field and a uniformly accelerated frame, in small enough regions of spacetime." [62]

and were very useful in physics, mathematics and geometry and could help the development of a quantum gravity theory (see [9]).

2.4.1 Sonic analog

Consider a non-relativistic fluid which is barotropic, irrotational and inviscid and is described by Euler's equation and the continuity equation [8]. As will become more clear later on, after linearizing the fluctuations describe a massless minimally-coupled scalar field with a d'Alembertian equation propagating in a (3+1)-dimensional Lorentzian geometry [51, 8]. Instead of refering to light cones, one can now better refer to so-called "propagation cones" where the speed of sound (or ripples,...) play the role of the speed of light [8]. Here, horizons form when the speed exceeds the speed of sound [8]. Or, when defining the Mach number as:

$$M = \frac{v}{c_s}, \tag{2.27}$$

when the Mach number is above unity [8]. So, a horizon is defined as the segment of space where [8]:

$$(\mathbf{v} \cdot \hat{n})_{\text{horizon}} = c_{s,\text{horizon}}, \text{ or } M_{\perp,\text{horizon}} = 1. \tag{2.28}$$

And thus a surface gravity, which represents the acceleration that a static observer close to the horizon undergoes observed from a observer at infinity, can be associated with it [8, 62, 9]:

$$\kappa = \left.\frac{\partial(c^2 - v^2)}{2\partial n}\right|_{\text{horizon}} = (c_s^2 \hat{n} \cdot \nabla M_\perp)_{\text{horizon}}. \tag{2.29}$$

Of course, a surface gravity can only be associated with a Killing horizon. However, we will not go any deeper into that topic [62]. For the interested reader, the complete derivation of the surface gravity is shown in [9]. Note that in Hawking's original paper [7], Einstein's equations were not used and thus, that the result can also be applied here, which gives for the Hawking temperature [8]:

$$k_B T_H = \frac{\hbar}{2\pi}(c_s \hat{n} \cdot \nabla M_\perp)_{\text{horizon}}. \tag{2.30}$$

This one is the analog model which can theoretically be explained best, and for that reason this one will be the subject of the next chapter and of this thesis [8]. Several other reasons why BECs are useful are due to the low speed of sound, low background temperature and the simplicity in inducing supersonic flow [8]. To extend on this topic, two types of acoustics can be considered: geometrical and physical acoustics [9]. In the case of geometrical acoustics, only the velocity of the fluid and the speed of sound should be well-defined [9]. On the other hand, the physical acoustics assume a irrotational, barotropic and inviscid fluid (cf. BEC) [8, 9].

2.4.2 Optical analog

In optics, when intense laser light, with a high enough electric field, is shined on a crystal than the refractive index can be modified [8]. This is called the *optical Kerr effect* and the exact equation is:

$$n = n_0 + \lambda K E^2, \tag{2.31}$$

with n_0 the refractive index of the crystal without light, λ the wavelength of the light, K the Kerr constant and E the electric field of the light [8]. This effect is also used in laser physics, to generate short pulses (e.g., Kerr-lens mode locking). In this way optical horizons can be constructed where the speed of the pulse is slower or faster in certain regions of the crystal [8]. In the rest frame of the photon, the perturbations move at different speeds [8]. There have been several experiments which have been performed on this topic [69, 70, 8]. When the laser beam hits the crystal, they measure the laser beam passing through but also other photons at other sides (perpendicular to the beam) [8]. This could be Hawking radiation, however this is not expected because the horizon is formed perpendicular to the beam and Hawking radiation is emitted perpendicular to the horizon [8]. Other effects could play a role, for instance, the dynamical Casimir effect or triboluminescence (breaking of electronic bonds, which produce light, when breaking crystal with e.g., a hamer) [8].

2.4.3 Surface waves

In the case of surface waves, it is more complicated, since shallow fluids should be considered ($\lambda \gg d$, with d the depth of the fluid) [8]. Here gravity waves should be considered which occur in fluids when gravity is the restoring force [8]. Then, the speed of the ripples are [8]:

$$c_s = \sqrt{g \cdot d}. \tag{2.32}$$

And now, similar to the sonic case, the Froude number should be considered [8]:

$$F = \frac{v_{\text{surface}}}{c_s}. \tag{2.33}$$

In this case, experiments have been performed (as in [71]). However, because the classical limit is considered, as opposed to the previous section, only the exponential Boltzmann factor is visible (but not the Planck spectrum) [8].

In this thesis yet another analog is considered (related to the sonic analog), based on using a Bose-Einstein condensate. Before developing the analogy, in the next chapter we first review the numerical techniques used to simulate Bose-Einstein condensates.

Chapter 3

Numerical techniques

In this chapter, the different numerical methods used to solve the Gross-Pitaevskii equation are shown. The pseudo-spectral split-step method is discussed and a method to include quantum fluctuations is discussed, called the truncated Wigner approximation (TWA)[72, 73, 74]. We also explain how to compute the most important observable used in this thesis, the density-density correlation function.

3.1 Pseudo-spectral split-step method

To numerically solve the Gross-Pitaevskii equation for a system, the pseudo-spectral split-step method is used. The time evolution needed is performed by Fourier transforming the wavefunction, evolve it in momentum space with the kinetic energy, inverse Fourier transforming and, lastly, evolving in real space with the potential ($\hbar = 1$):

$$\psi(x) \xrightarrow{\mathscr{F}} \psi(k) \to e^{-idt\frac{k^2}{2m}}\psi(k) \xrightarrow{\mathscr{F}^{-1}} \psi(x) \to e^{-idt(V+g|\psi(x)|^2)}\psi(x) = \psi^{'}(x) \tag{3.1}$$

A reason to use small time steps, is because for operators, the exponentials cannot be split. However, when the time steps are small (cf. the derivation of the path integral formulation from Schrödinger's quantum mechanics), the exponentials can be split as in the Trotter product formula, which is especially used for the simulation of Hamiltonian dynamics,:

$$e^{\lambda(\hat{T}+\hat{V})} = \lim_{N\to\infty}(e^{\lambda\hat{T}/N}e^{\lambda\hat{V}/N})^N, \tag{3.2}$$

with λ an arbitrary parameter. Otherwise, the action of the kinetic energy and potential energy is performed at once and no Fourier transform can be used such that the kinetic energy can act easier on the wavefunction.

Before starting the time evolution, an initial wavefunction is needed. As an initial state we choose a condensate in a (one-dimensional) box potential (two

hard walls confine the atoms). A good guess for the wave function in this case takes the form of a product of tangent hyperbolic functions that let the density heal from zero at the wall towards the bulk density over a distance given by the healing length. Then, an imaginary time evolution is performed to relax this initial guess to the true ground state for the box potential. The wavefunction can be seen as the sum of eigenstates where the amplitude of the eigenstates decrease over time, when time is replaced with imaginary time, and the ground state decreases the slowest [75]. So, by changing the wavefunction each time, the ground state will be found [75].

3.2 Truncated Wigner Approximation

The truncated Wigner approximation (TWA) is a phase space method and can be seen as a stochastic generalization of the Gross-Pitaevskii equation. It accounts for the quantum fluctuations by only adding some noise to the initial state [76]. In the TWA, an ensemble of wavefunctions is created which are sampled from the Wigner quasiprobability distribution. Each member of the ensemble is propagated over time using the Gross-Pitaevskii equation. Expectation values of observables are then found by averaging over the time-evolved ensemble. Whereas the Gross-Pitaevskii equation only captures the mean-field evolution, the ensemble averaging adds the effect of quantum fluctuations.

3.2.1 The Wigner quasiprobability distribution

In the seminal work of Eugene Wigner from 1932 [72], the Wigner distribution was introduced to study quantum corrections to the Boltzmann equation from thermodynamics/statistical mechanics. Nowadays, it can be applied to many problems in quantum mechanics, because it is an alternative formulation of Schrödinger's quantum mechanics called the phase-space formulation of quantum mechanics [77]. As an example, a single-mode quantum system is discussed. This section is based on [47].

The characteristic function of the density matrix is defined as:

$$\chi(\lambda, \lambda^*) = \mathrm{Tr}\left(\hat{\rho} e^{\lambda \hat{a}^\dagger - \lambda^* \hat{a}}\right). \tag{3.3}$$

The Wigner quasiprobability distribution is the Fourier transform of the characteristic function [73]:

$$W(\alpha, \alpha^*) = \frac{1}{\pi^2} \int e^{-\lambda\alpha^* + \lambda^*\alpha} \chi(\lambda, \lambda^*) d^2\lambda, \tag{3.4}$$

which is also normalized:

$$\int W(\alpha, \alpha^*) d^2\alpha = 1. \tag{3.5}$$

The reason why it is called a *quasi*probability distribution is because it can have negative values. Frequently, for our purposes, the Wigner quasiprobability

distribution can be approximated to be close to a Gaussian. For Bose gases, the dynamics of the Wigner quasiparticle distribution, when neglecting the third order derivatives (therefore, it is called the Truncated Wigner Approximation (TWA)), can be sampled by evolving the bosonic field according to the Gross-Pitaevskii equation, as noted in [73]. In order to avoid infinities, which arise from the commutator $[\hat{\psi}(r), \hat{\psi}(r)^\dagger] = \delta(0) = \infty$, one actually has to study the following discretized Hamiltonian, for which $[\hat{\psi}(r_i), \hat{\psi}(r_j)^\dagger] = \delta_{ij}/dV$,:

$$\mathcal{H} = \sum_k \frac{\hbar^2 k^2}{2m} \hat{a}_k^\dagger \hat{a}_k + dV \sum_r U(r)\hat{\psi}^\dagger(r)\hat{\psi}(r) + \frac{g}{2} dV \sum_r \hat{\psi}^\dagger(r)\hat{\psi}^\dagger(r)\hat{\psi}(r)\hat{\psi}(r), \tag{3.6}$$

with dV the volume of a unit cell of the grid and $U(r)$ is the trapping potential [73]. The divergence arised from the addition of noise with each mode, where the number of modes are infinite [73]. The discretisation is performed by expanding the wavefunction in plane waves:

$$\hat{\psi}(r) = \frac{1}{\sqrt{V}} \sum_k \hat{a}_k e^{ikr}, \tag{3.7}$$

where the wavenumber k takes on values in the Brillouin zone corresponding to the discrete lattice. with $\hat{a}_k$ the annihilation operator for k [73].

3.2.2 Initial state preparation

For dilute Bose gases ($n\xi \gg 1$), the TWA approach and the time-dependent Bogoliubov approach are equivalent, where for TWA, longer-time studies can be performed, as mentioned in [16]. The initial state of our system is at mean field (Gross-Pitaevskii) level:

$$\psi_0(x) = e^{i(k_0 x - \omega_0 t)} \sqrt{n_0}. \tag{3.8}$$

In the TWA, noise is added to it according to:

$$\psi_0(x) = e^{i(k_0 x - \omega_0 t)} \frac{1}{\sqrt{L}} \left(\sqrt{n_0} + \sum_{k \neq 0} (\alpha_k u_k e^{ikx} + \alpha_k^* v_k e^{-ikx}) \right), \tag{3.9}$$

where L is the length of our system. α_k are random variables, which for our simulation, are chosen to be gaussian and independent of each other [16]. The mean is zero and the variance depends on the temperature:

$$\langle \alpha_k \rangle = \langle \alpha_k^2 \rangle = 0, \tag{3.10}$$

and

$$\langle |\alpha_k|^2 \rangle = \frac{1}{2 \tanh\left(\frac{\epsilon_k}{2k_B T}\right)}, \tag{3.11}$$

with $\epsilon_k = \sqrt{E_k(E_k + 2gn)}$ the Bogoliubov dispersion and $E_k = \frac{\hbar^2 k^2}{2m}$ [16]. The probability distribution is correspondingly [73]:

$$P(\alpha_k) = \frac{2}{\pi} \tanh\left(\frac{\epsilon_k}{2k_B T}\right) e^{-2|\alpha_k|^2 \tanh\left(\frac{\epsilon_k}{2k_B T}\right)}. \tag{3.12}$$

In our system, the temperature is zero and the variance approaches 1/2. The Bogoliubov coefficients are defined by the following equations [16]:

$$u_k + v_k = (E_k/\epsilon_k)^{1/4}, \tag{3.13}$$

$$u_k - v_k = (E_k/\epsilon_k)^{-1/4}. \tag{3.14}$$

3.2.3 Evolution and disadvantages

The previously prepared initial wavefunctions will then evolve using the Gross-Pitaevskii equation. Finally, the results will be the average over the final wavefunction ensemble. Of course, this method has several disadvantages. First of all, this is of course never *exact*: a large ensemble is needed which may be computationally expensive. Also, the grid used for the simulations is always finite and will never replicate the exact dynamics. Finally, in the *truncated* Wigner approximation, the cubic derivatives of W are neglected to retrieve the Gross-Pitaevskii dynamics. This neglects effects such as 'quantum jumps'. However, this is a simple and relatively good method for now.

For a more extensive overview of the truncated Wigner method and its advantages and applications, see [78].

3.3 Density correlation function

The power loss due to Hawking radiation for astrophysical black holes is immeasurably small (10^{-48} W), and so cannot be measured [8, 9]. Nevertheless, the advantage is that in a BEC, one has access to both sides of the horizon and thus can measure possible correlation between both the Hawking and Partner particles [8, 9]. And so, the density-density correlation function is an important observable for the detection of Hawking radiation. It is defined as [79]:

$$G^{(2)}(x, x') = \frac{\langle \hat{\psi}^\dagger(x)\hat{\psi}^\dagger(x')\hat{\psi}(x')\hat{\psi}(x)\rangle}{\langle \hat{\psi}^\dagger(x)\hat{\psi}(x)\rangle \langle \hat{\psi}^\dagger(x')\hat{\psi}(x')\rangle}. \tag{3.15}$$

The normally ordered quantities which are used for the calculation of the density-density correlation function are [79]:

$$\begin{aligned}\langle \hat{\psi}^\dagger(x)\hat{\psi}^\dagger(x')\hat{\psi}(x')\hat{\psi}(x)\rangle &= \langle |\psi(x)|^2 |\psi(x')|^2\rangle_W \\ &+ \frac{1}{4\Delta x^2}(1 + \delta_{x,x'}) - \frac{1}{2\Delta x}(1 + \delta_{x,x'})\langle |\psi(x)|^2 + |\psi(x')|^2\rangle_W,\end{aligned} \tag{3.16}$$

and

$$\langle \hat{\psi}^\dagger(x)\hat{\psi}(x)\rangle = \langle |\psi(x)|^2\rangle_W - \frac{1}{2\Delta x}. \tag{3.17}$$

For Bose gases without a time-dependent potential, there is only a diagonal line visible which is a result of many-body anti-bunching. The latter is related to the repulsive interactions between the bosons. In a Fermi gas however, there is nothing on the diagonal because of the Pauli exclusion principle.

In the next chapter, this will be worked out in more detail for the case of a step horizon, as used in the analogy for Hawking radiation.

Chapter 4

Hawking radiation and other excitations

Hawking radiation has a temperature that is very low, which is very complicated to measure in an enviroment with a higher background temperature. To circumvent this issue, an analogy can be made between Black Holes and Bose-Einstein condensates. This will be further discussed below. From this, it is possible to simulate the behavior of a BEC with a sharp potential step which sweeps through the condensate. Also, the experimental side will be addressed (the RuBECi setup). Other setups will be explored theoretically, including the oscillating horizon experiment.

4.1 Introduction

Consider the sonic black hole configuration as shown in Figure 4.1. The BEC is flowing in the positive x-direction and the horizon is located at $x = 0$ [80]. A sharp potential step is placed at $x = 0$ [80]. This results in two parts of the system: the left side (upstream region) is the subsonic region and the right side (downstream region) is the supersonic region [80]. This corresponds to the event horizon in gravitational black holes, because a sound wave in the downstream region cannot travel against the flow and will be dragged away in the downstream region [80]. The Hawking radiation can be measured using the density correlation function (as in [80]), because two correlated excitations are produced which travel in the opposite direction. This should give a anti-diagonal line on the density correlation function. The Hawking radiation has been claimed to be measured by Steinhauer et al [22].

A more detailed mathematical explanation can be given. This is based on [51]. Consider density and phase fluctuations of the wavefunction:

$$\Psi(\mathbf{r},t) = e^{-i\mu t/\hbar}\Psi_0(\mathbf{r})[1+\phi(\mathbf{r},t)] = e^{-i\mu t/\hbar}\sqrt{n}e^{i\Theta}\left[1+\frac{n_1}{2n}+i\Theta_1\right], \quad (4.1)$$

with the total density being $n = n_0 + n_1$ and for the total phase $\Theta = \Theta_0 + \Theta_1$. Filling these into the hydrodynamic equations (see Chapter 2), gives:

$$\partial_t n_1 + \nabla \cdot (n_1 \mathbf{v} + n_0 \hbar \nabla \Theta_1 / M) = 0, \tag{4.2}$$

$$\hbar \partial_t \Theta_1 + \hbar \mathbf{v} \nabla \Theta_1 + g n_1 - \frac{\hbar^2}{4Mn} \nabla \cdot (n \nabla (n_1/n)) = 0. \tag{4.3}$$

The velocity here is the velocity generated by the phase Θ_0. In the long wavelength limit, where the momenta are small and the dispersion relation is linear such that the analogy with the speed of sound can be made, the density variation reduces to:

$$n_1 = -\frac{\hbar}{g}(\partial_t \Theta_1 + \mathbf{v} \cdot \nabla \Theta_1), \tag{4.4}$$

and the phase fluctuation obeys the following equation:

$$-(\partial_t + \nabla \cdot \mathbf{v}) \frac{n_0}{M c_s^2} (\partial_t + \mathbf{v} \cdot \nabla) \Theta_1 + \nabla \cdot \left(\frac{n_0}{M} \nabla \Theta_1 \right) = 0. \tag{4.5}$$

This equation can be brought in the form of a d'Alembertian[1] with a corresponding metric, which belongs to a conformal class of Lorentzian metrics [9]:

$$\Box \Theta_1 = \frac{1}{\sqrt{|g|}} \partial_\mu (\sqrt{|g|} g^{\mu\nu} \partial_\nu \Theta_1) = 0, \tag{4.6}$$

$$g_{\mu\nu} = \frac{n_0}{c_s} \begin{bmatrix} -(c_s^2 - v^2) & -v^j \\ -v^i & \delta_{ij} \end{bmatrix}. \tag{4.7}$$

Thus, "Phase fluctuations in the Bose-Einstein condensate can be interpreted as a minimally-coupled massless scalar field propagating in a (3+1)-dimensional Lorentzian geometry", as noted in ref. [51]. So, here the fixed speed of sound takes over the role of the speed of light in black holes. This is the idea of Analog Gravity.

There are different parts of the life of a "dumb" (or sonic black) hole: the ramp-up, spontaneous, multi-mode and mono-chromatic modes [81]. The last two occur only in the case of the creation of the inner horizon [81]. In the case of spontaneous Hawking radiation, the radiation is stationary [81]. Here, only spontaneous Hawking radiation is considered. In that case, entanglement between the Hawking pairs can be detected (except at low wavenumbers, where it can be destroyed) [22, 21]. In the case of an inner horizon, stimulated Hawking radiation can be found which could function as a black hole lasing, however, this is still unsure (as it could be Bogoliubov-Cherenkov-Landau stimulated Hawking radiation) [19, 81, 20].

[1] The conventional tensor notation is used: Greek indices are used as space-time indices running from 0 to 3, Latin indices are used as space indices running from 1 to 3, and the Einstein summation convention is assumed.

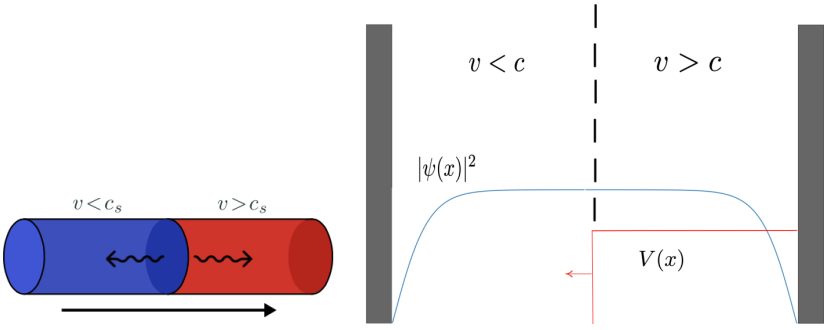

Figure 4.1: The flow is in the positive x-direction [80]. A sharp potential step is placed at $x = 0$ [80]. This splits the system into two parts: the left side (upstream region) is the subsonic region and the right side (downstream region) is the supersonic region [80]. The wiggly lines in the first figure represent the Hawking radiation [51]. For the second figure, the potential and density is plotted (not on scale). A spatially-dependent g is used (which will be explained later). The density stays constant, then. So, the speed of sound is different for the $x > 0$ and $x < 0$. Source: [51]

4.2 Numerical remarks

The implementation of the initial state in MATLAB (see script in appendix A) is done as follows. The random variables α_k are implemented as a complex variable with real and imaginary parts random numbers which are normally distributed with mean 0 and standard deviation $1/\sqrt{2}$. This is performed by the `randn` command in MATLAB. For the time evolution, the split-step method is used and imaginary time evolution is applied to retrieve the initial ground state (this has not that big of an effect, only at the edges it makes the order parameter smoother). In what follows, we use units such that $\hbar = m = \xi = 1$, where ξ is the healing length corresponding to the average density.

4.3 Testing the script

As a first case to consider, the potential is turned off. Here, the momentum distribution of particles is

$$n_k = \sum_{i=1}^{N} |\Psi_i(k)|^2 - 1/2, \tag{4.8}$$

where N stands for the number of wavefunctions in the ensemble, should be the same before and after the time evolution via the GPE. The $-1/2$ is a result of

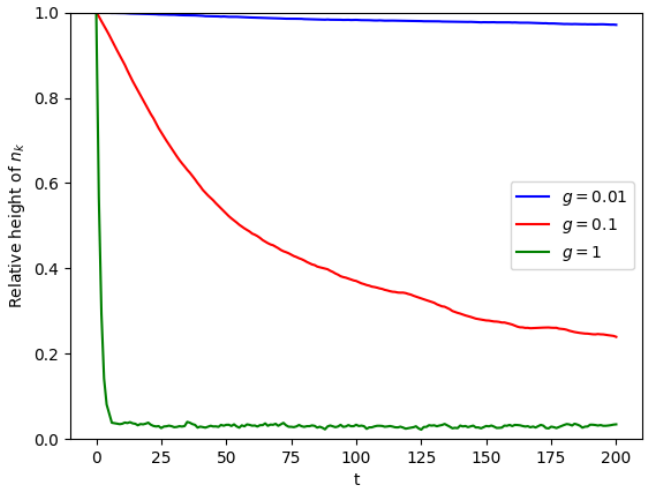

Figure 4.2: The intensity of the condensate mode in the momentum distribution as a function of the evolution time for several values of the interaction strength g. The lower the interaction strength, the more stable the condensate is. The height is normalized against the peak value at time zero. Here $\hbar = 1$ and $m = 1$.

the vacuum contribution to the density in the truncated Wigner method. This is performed as a first test of the script. Now, for the case of a 'large' interaction strength (of the order 1), the condensate decays and gets destroyed. In addition, the Gross-Pitaevskii equation may not be valid anymore. This can be seen by evaluating the peak height at $k = 0$ (the ground state, which should be macroscopically occupied). The lower the interaction strength, the more stable the condensate is. In Figure 4.2, the height of the condensate mode is plotted as a function of the evolution time for several different values of g. Moreover, the momentum distribution also agrees with the Bogoliubov result apart from the trivial quantum depletion at $k = 0$. Also, the decay of the condensate is not important because for realistic values, using rubidium-87 atoms, there is no sign of decay. In this case, the density-density correlation function only shows a diagonal $x = x'$ line which is a result of many-body antibunching, which in turn is a result of the repulsive interactions between the atoms [16].

4.4 Step-sweep experiment and the experimental feasibility

As explained in the previous sections, the analog of a horizon can be reached by using a potential step. Now, to simulate the flow of the condesate, the step is moved with a speed v which is chosen to be in between the speed of sound at both

sides of the horizon. A initial density plot is shown in Figure 4.1.However, the Bogoliubov spectra, which is used for the noise in the truncated Wigner method, is not applicable anymore in this case. A general way to solve for the dispersion is by solving the Bogoliubov-de Gennes equations which is challenging. To avoid this problem, the step is turned on at a finite time greater than zero. In this way, the noise for the homogeneous system can be used for the initial condition. In the presence of the moving step, the density-density correlation function shows some interesting features. However, the parts at both sides of the diagonal line should not be mistaken for Hawking radiation. They could possibly come from a shock wave, which originated from the sudden switch-on of the potential step. This shock wave results in a false signal of correlated Hawking particles. This is similar to the soliton shedding mentioned in [16]. To minimize these effects the interaction constant g varies such that the Hartree energy $V + gn$ stays constant [16].

Now, to create an interaction strength modulation experimentally is challenging. In the RuBECi setup (discussed in more detail in chapter 5) one can for example change the confinement in the y-direction which results in a change in g which compensates for the change in density. The Hartree energy is $V(x) + gn + E_0$, where E_0 can represent zero-point energy that may or may not depend on position.

The interaction strength in an effective 1D Bose-Einstein Condensate depends on the s-wave scattering length but also on the parameters of the tight confinement in the "frozen out" directions. In our case, we assume a harmonic confinement potential.

Firstly, the easier case of a cylindrically symmetric transverse trap will be studied. In this case, the wavefunction may be split into two parts, a longitudinal and transverse part [75]:

$$\Psi(x, y, z) = \psi(x)\Phi(y, z). \tag{4.9}$$

After plugging this into the Gross-Pitaevskii equation, the effective interaction strength becomes (assuming the ground state wavefunction of a harmonic potential still holds, regardless of the quantum noise):

$$g = 2\hbar a_s \omega_\perp, \tag{4.10}$$

with zero-point energy of $\hbar\omega_\perp$ [75].

Consider the Hartee or mean-field energy:

$$E_{\mathrm{MF}} = V(x) + gn + \hbar\omega_\perp. \tag{4.11}$$

Entering the equation for the effective interaction strength in the above equation results in:

$$E_{\mathrm{MF}} = V(x) + 2\hbar\omega_\perp a_s n + \hbar\omega_\perp. \tag{4.12}$$

Solving for $\omega_\perp$ gives:

$$\omega_\perp(x) = \frac{E_{\mathrm{MF}} - V(x)}{\hbar(1 + 2a_s n)}. \tag{4.13}$$

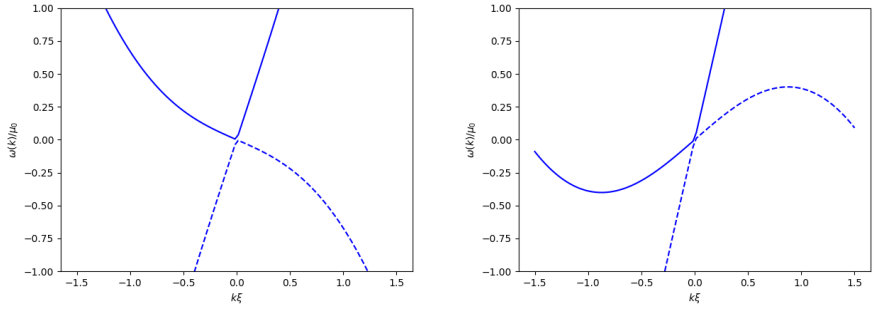

Figure 4.3: The dispersion relation in the case of $v/c = 0.75$ and $v/c = 1.5$. For the first figure, the top left line can be denoted as the 'alpha' branch (actually, it is the straight line which serves as a tangent). In the second figure, the tangent to the full line at the left is the 'beta' branch and the tangent to the full line at the right is the 'gamma' branch. Based on: [16].

The implementation gives the result shown in Figure 4.4. On the top right corner, there is a bit of a checkerboard pattern visible due to numerical instabilities. This is because, the lower the grid size the smaller the checkerboard pattern becomes. So, this is purely an effect which arises from numerical discretization and edge effects could also play a role. Still, the results are the same as in [16]. The fringes in the upper right half come from the dynamical Casimir effect, due to the spontaneous change in the interaction strength [16]. The dynamical Casimir effect is an extension of the static Casimir effect discussed in the next chapter, in which a sudden change of boundaries or certain system parameters (in this case, the interaction strength) can result in the production of a pair of particles (the two opposite fringes).

The remaining two lines in Figure 4.4, in the lower left part, can be interpreted as follows. The dispersion relation can be writen as (with $\hbar = m = 1$) [80]:

$$\omega = vk \pm \sqrt{\frac{k^2}{2}\left(\frac{k^2}{2} + 2gn\right)}. \tag{4.14}$$

In the case of subsonic flow ($v/c = 0.75$), the dispersion relation is plotted in the left panel of Figure 4.3. The supersonic flow case ($v/c = 1.5$) is shown in right panel of Figure 4.3. Now, the Hawking radiation will follow the alpha and beta branches with different speeds [16]. The phonon from the alpha branch will be followed by a speed of $v - c_1$ (the left side of the horizon) and the phonon from the beta branch will be followed by a speed of $v - c_2$ (the right side of the horizon) [16]. This results in a slope of the corresponding line on the density correlation function which is $(v - c_1)/(v - c_2)$ [16]. Of course, the alpha branch may partially back-scatter to the gamma branch which is 'traversed' by a speed $v + c_2$ [16]. So, this will result in an additional line with slope $(v - c_2)/(v + c_2)$

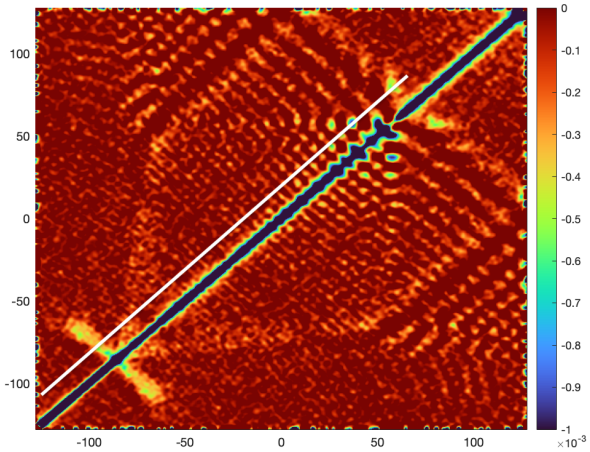

Figure 4.4: The density-density correlation function, in the case of a moving step potential and varying interaction constant (but with an experimentally changing $\omega_\perp$). The results are similar to the ones in [16]. The units of position are such that the healing length is 1. The white line indicates a cut which will be used in Figure 4.5.

[16]. Now, a quantitative analysis can be performed. A small cut, parallel to the diagonal line gives the result shown in Figure 4.5. The first Hawking mode can be seen to be at -96 and the second Hawking mode (is just visible) is at -82. Also, the evolution of the length of the first Hawking line is plotted in Figure 4.6. It grows linearly. The speed corresponding to this is 0.2 which is the highest speed of sound (0.7) minus the speed of the horizon (0.5). This is not a coincidence. The sound waves corresponding to the line should first 'catch up' with the horizon and, also, 'enlarge' the line. So, the speed at which the line enlarges is $0.7 - 0.5 = 0.2$, as expected. In addition, the correlation function was plotted in the case of temperature. Edge effects play a role in this, however, they are removed from the figure (cutting them out). As can be seen, there is a third line which comes from the thermal phonons which reflect from the horizon [16].

4.5 The de Laval nozzle

A different experimental setup can be studied, which is called the de Laval nozzle. The name is misleading; it is generally used to convert thermal heat into a directed propulsion. However, the geometric shape is similar. This nozzle has three regions: subsonic, supersonic and again subsonic. This can classically be modelled by using a pipe which has a smaller diameter at the regions of

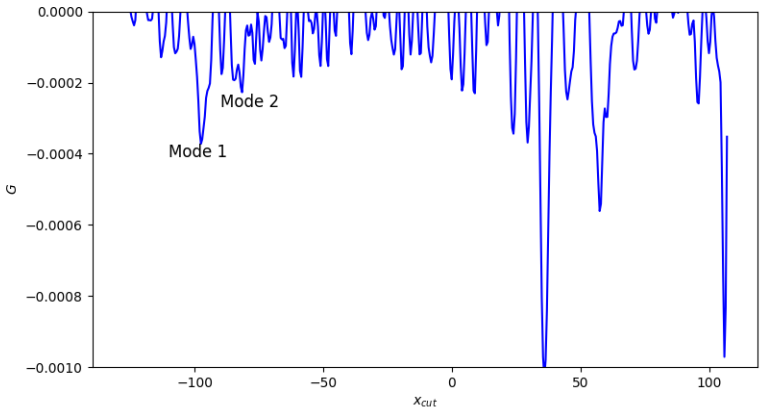

Figure 4.5: A cut taken parallel to the diagonal line of the density-density correlation function. The line through which the cut is taken is shown, approximately, on Figure 4.4.

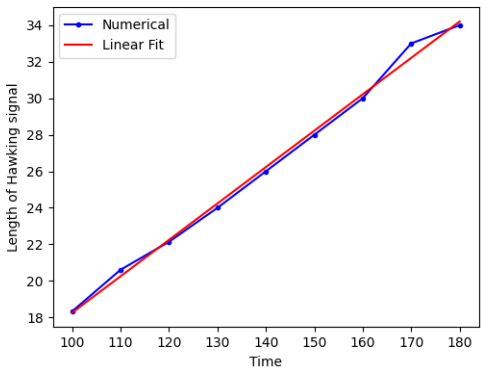

Figure 4.6: Time evolution of size of the first Hawking line in the correlation function. The speed is 0.2.

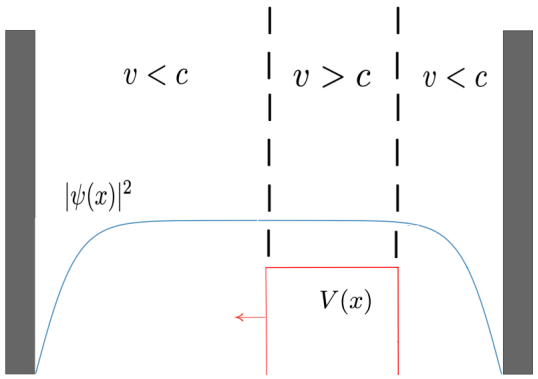

Figure 4.7: An illustration of the implementation that is used to create the de Laval nozzle setup in a condensate. To obtain the alternation of subsonic, supersonic and subsonic regions as suggested in Ref. [82] a moving step potential is used.

transition. The flow becomes 'enhanced' and the speed increases. After going through the second constriction the speed gets subsonic again. An illustration is shown in Figure 4.7. This is an interesting situation to model, because it results in two horizons which may cause the Hawking radiation to self-amplify and thus constitute a so-called 'black-hole laser' [19]. This can be modelled by using a potential 'mountain' instead of a single step. In this case, two horizons are present and this should result in a checkerboard pattern as in [19] where the horizontal and vertical lines may indicate stimulated Hawking radiation. The density-density correlation function is shown in Figure 4.8. The Hawking radiation in this setup is comparable to the Hawking radiation in the previous setup. The setup which has two horizons does not add any extra value to the detection of Hawking radiation.

4.6 Bragg spectroscopy

The spectra of excitations for certain systems can be studied using Bragg spectroscopy [83]. In this case, a Bragg pulse is added to the potential:

$$V_{Bragg} = Ae^{-(t-t_0)^2/(2\sigma_t^2)}e^{-(x-x_0)^2/(2\sigma_x^2)}\cos[kx - \omega(t-t_0)], \tag{4.15}$$

with A the amplitude, k the wavenumber, ω the frequency, σ_t the spread of the wavepacket in time-domain (chosen to be large) and σ_x the spread of the wavepacket in real space. When applying such a Bragg pulse to a condensate, the $n_k(t)$ has a peak at the wavenumber of the pulse. The amplitude of this

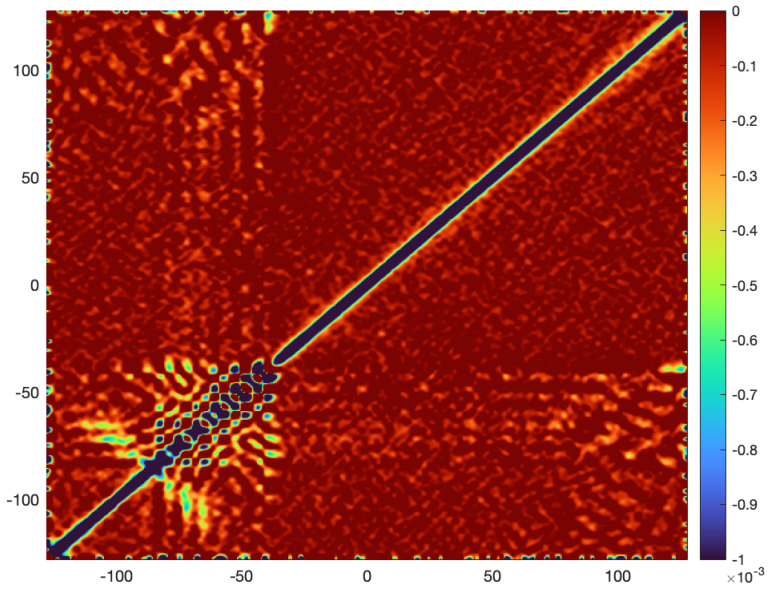

Figure 4.8: The density-density correlation function in the case of a de Laval nozzle with two horizons. The result is similar to [19].

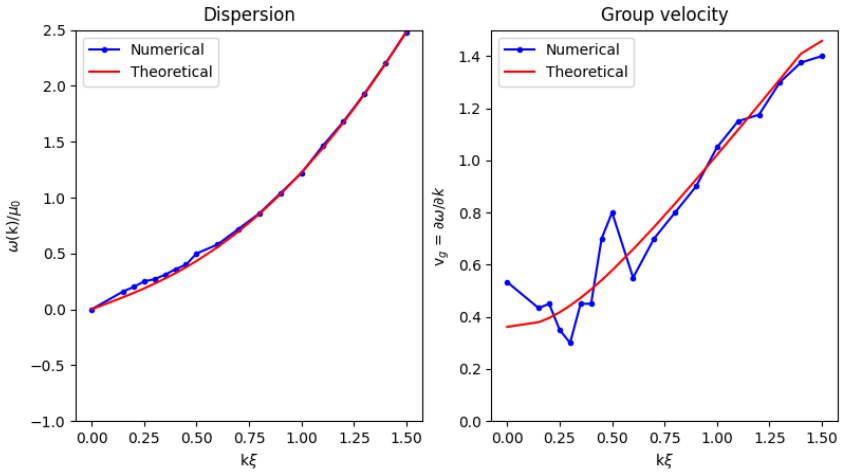

Figure 4.9: The dispersion and group velocity for a homogeneous condensate calculated using Bragg spectroscopy (numerical) and the Bogoliubov dispersion (theoretical).

peak depends on the frequency of the pulse. The maximum amplitude of the peak is at the eigenfrequency frequency (which follows the dispersion).

4.6.1 Dispersions

Homogeneous condensate

In the case of a homogeneous condensate without a horizon, the dispersion should be the familiar Bogoliubov dispersion. So, for several k values, the optimal ω values were found and plotted as shown in Figure 4.9. They almost perfectly fit with the Bogoliubov dispersion relation for the chosen g. The group velocity can also be calculated by using a gradient. The gradient calculated by using the numerical data contains jumps which are expected, because the data is noisy. The numerical errorbar is determined by the grid size.

Horizon with no velocity

In the case of an inhomogeneous condensate (in this case, with an horizon), there are two parts of the condensate with 'different' dispersions. At the right side (the one studied here), the g is different from the previous paragraph. The dispersion can still be fitted by using a Bogoliubov dispersion with a changed g. The results are shown in Figure 4.10. This is only for $x > 0$, because for $x < 0$ it is still the same as in the previous paragraph.

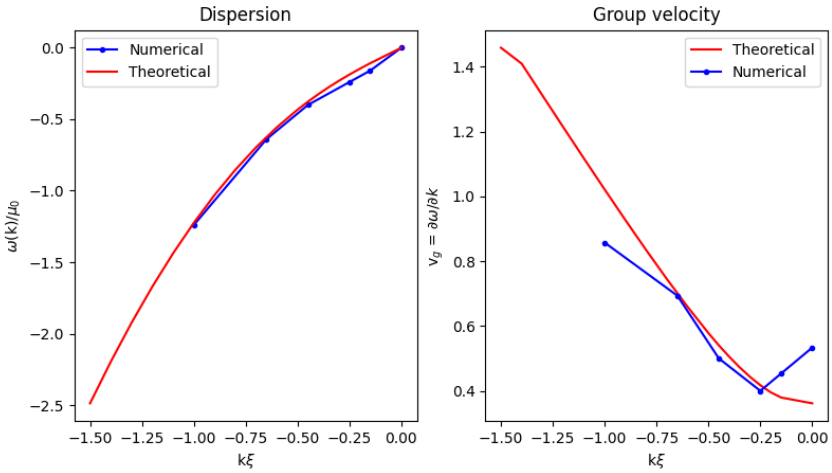

Figure 4.10: The dispersion and group velocity for a condensate with a horizon with zero speed, calculated using Bragg spectroscopy (numerical) and the Bogoliubov dispersion (theoretical).

Moving horizon

The case of an inhomogeneous and moving condensate is a bit different then the previous ones. The found values of ω can be linked to those of the static horizon by transforming to a frame of reference co-moving with the horizon. In this case, as can be seen from Figure 4.11 , the results coincide. The change in sign comes from taking into account the direction in which the Bragg pulse is moving. Again, the numerical and theoretical results agree.

4.6.2 Transimission and reflection

In this part, the transmission and reflection of these Bragg pulses against the horizon will be studied

Without mean speed

In this case, as can be seen from the dispersion, there are only 2 modes: the one which got transmitted and one which got reflected. The smoother the horizon, the smaller the amplitude of the reflected wave becomes. In Figure 4.12, the change in density is shown. The potential and difference in density are not on the same scale. A transmitted and reflected wave is seen.

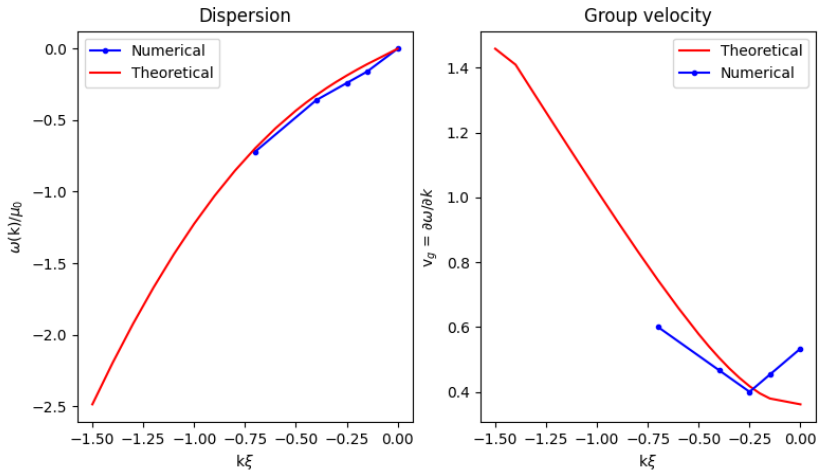

Figure 4.11: The dispersion and group velocity for a condensate with a horizon with a mean speed, calculated using Bragg spectroscopy (numerical) and the Bogoliubov dispersion (theoretical). The Doppler shift is not shown here, in both cases.

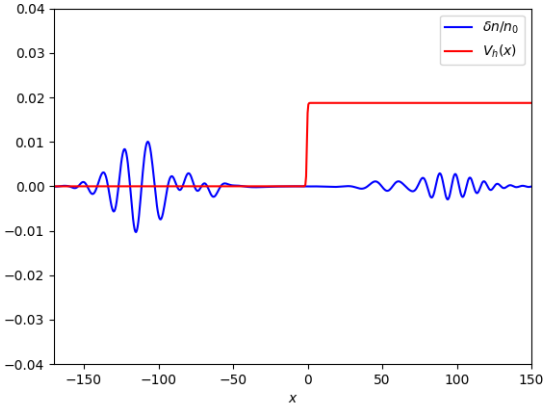

Figure 4.12: The transmission and reflection of the Bragg pulse in the density, for the case of a -non moving- horizon, is shown. The potential form (not on scale) is also shown.

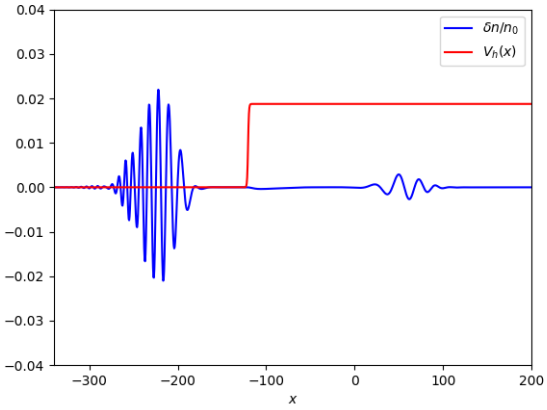

Figure 4.13: The transmission and reflection of the Bragg pulse in the density, for the case of a moving horizon, is shown. The potential form (not on scale) is shown, as well .

With mean speed

In the case of a net speed, the change in density is shown in 4.13. A transmitted and reflected wave is shown. Also, another (small) transmitted wave is seen (at approximately -300). The three wavevectors seen on the Fourier transform are 0.47, 0.4 and 0.16. The ratio between 0.47 and 0.16 is expected (close to $(v_0 - c_1)/(v_0 + c_1)$, as noted in [84]). The speed of the reflected wave is also the same as the expected one.

4.7 Oscillating horizon experiment

Let us now consider a step potential with a perodic oscillating motion superimposed on a constant velocity. So, the horizon position is:

$$x_{\rm pos} = -vt + A\sin(\omega t). \tag{4.16}$$

In this case, correlated waves are created. In the density-density correlation function, fringes are now created, as shown in Figure 4.14.

The distance between the fringes agrees with the frequency of oscillation. Actually, there would be an asymmetry in the density-density correlation function because the frequency of excitations differ on both sides of the horizon because the interaction strength is different on both sides. This is a bit visible because the line is not exactly parallel to the diagonal line. Note that, the density-density correlation function in the figure is created by using a bit different values than the previous figures. The previous figure used 50 for the density and the range for the interaction strength is 0.01 to 0.0025. For the

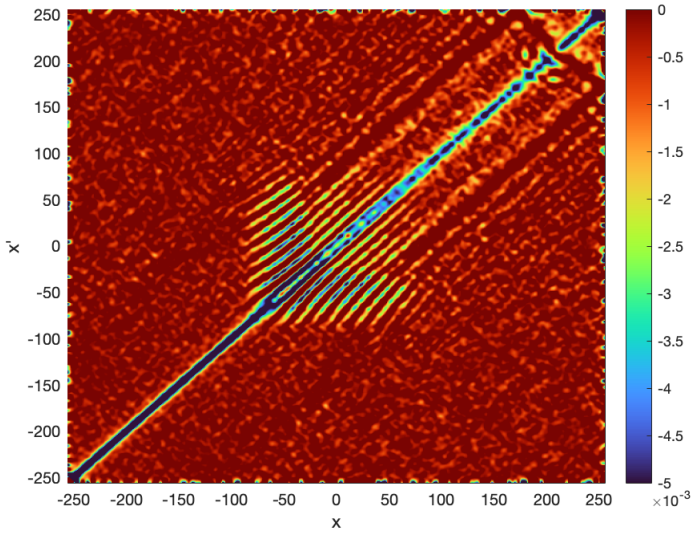

Figure 4.14: The density-density correlation function in the case of an oscillating horizon and a sweep.

current figure, the density is 8.35 and the interaction strength goes from 0.013 to 0.0032.

The asymmetry has been confirmed where the ratio between the two end point distances are, approximately, 1.86. The difference with the theoretically calculated wavelengths (using the dispersion) is a factor 4 which comes from the definition of a density correlation function. The wavefunction can be represented as:

$$\psi(x) = \psi_0(x) + C(\alpha u e^{ikx} + \alpha^* v e^{-ikx}), \tag{4.17}$$

with C a constant and α a random complex Gaussian number. When looking at the numerator of G, four factors containing e^{i4kx} can be extracted with prefactor $|\alpha|^4|u|^2|v|^2$ which, after averaging, is not zero. The denominator has as highest power 1 because other combinations such as $\alpha\alpha$ and $\alpha^*\alpha^*$ give zero, after averaging.

In the case of a purely oscillating horizon, with the $v = 0$ in 4.14, i.e. without a sweep, we have not observed any visisble Hawking radiation in our numerics for the density-density correlation function.

This may be because a Bose-Einstein condensate is only superfluid at velocities lower than a critical velocity (sound velocity). This is a version of Landau's superfluidity criterion. In the case of an oscillating horizon experiment the problem is that the speed is only larger than the perturbation speed for a short time because the speed v goes back to zero and then changes sign. If the speed is larger than both sound speeds, at both sides the speed becomes larger than the perturbation speed and multiple sonic booms are made. This can be supported

by the fact that the fringes are created when the horizon moves with negative velocity v.

Apart from looking into Hawking radiation, we are also curious at other excitations. In that case, the velocity related to the oscillation is set to be larger than both sound velocities. This gives fringes related to excitations.

4.8 Summary

In this chapter a variety of results were presented, so it can be useful to summarize and group our findings.

- We simulated the potential step sweep experiment of Steinhauer. The Truncated Wigner approximation was used to capture the effects of quantum fluctuations. In order to suppress noise from phonons and shock waves, the interaction strength is modulated to keep the Hartree energy fixed. We identified the Hawking radiation, and have characterized its propagation, and discussed temperature effects.

- Several alternative setups were investigated, namely an oscillating horizon and a Laval nozze setup with two horizons. Although these also exhibit Hawking radiation, the detectability of the radiation is not significantly improved.

- The use of Bragg pulses to study the horizon was also investigated. These excitations are used experimentally to study the spectrum of condensates, and are seen to interact with the artificial event horizon. The scattering of the Bragg pulse at the horizon was characterized.

Hawking radiation is not unique in revealing quantum fluctuations. In the context of an ongoing collaboration between UGhent and Universiteit Antwerpen, we investigated another effect of quantum fluctuations, the static Casimir effect mentioned in the introduction. In the next chapter, we turn our attention to the question of its detectability in Bose condensates.

Chapter 5

Static Casimir effect

In this chapter, the Casimir effect will be discussed for the case of BECs and an order of magnitude estimate will be made for an experimental setup that is quasi-1D, such that one knows if it is possible to measure it for this particular system. Moreover, the case of multiple plates is ratiocinated.

5.1 The Casimir force in a 1D BEC

The derivation of the Casimir force for the case of a quasi-one-dimensional BEC is based on [17]. From now on the following units are used (unless explicitly stated): $\hbar = 1$, $2m = 1$ and $k_B = 1$ [1] [17].

The Hamiltonian for a three-dimensional dilute Bose gas can be adapted such that it describes a quasi-one-dimensional dilute Bose gas, by introducing an isotropic two-dimensional harmonic potential [17]. The effective Hamiltonian then becomes:

$$H_{\text{eff}} = -\sum_{i=1}^{N} \nabla_i^2 + g \sum_{i<j} \delta(r_i - r_j) \frac{\partial}{\partial r_{ij}} r_{ij} + \sum_i \frac{1}{4} \omega_\perp^2 r_{i\perp}^2, \tag{5.1}$$

where $r_{i\perp} = y^2 + z^2$ and $\omega_\perp^2$ stands for the frequency of the harmonic potential well [17]. If the potential is strong enough such that the two (y and z) degrees of freedom of the atoms will be frozen, an effective 1D Hamiltonian can be constructed (with a renormalized interaction strength $g_{1\text{D}} = \frac{g}{\pi a_\perp^2} \left(1 - C \frac{a}{a_\perp}\right)^{-1}$):

$$H_{\text{eff}}^{1\text{D}} = -\sum_{i=1}^{N} \frac{\partial^2}{\partial r_i^2} + g_{1\text{D}} \sum_{i<j} \delta(r_i - r_j) \frac{\partial}{\partial x_{ij}} x_{ij}, \tag{5.2}$$

where $a_\perp = (\hbar/(m\omega_\perp))^{1/2}$ the characteristic length of the harmonic trap and $C = 1.4603...$ a constant [17]. Note that now (compared to the 3D case) the

[1] Note that in this section m is used for the reduced mass while later it will be used as the "actual" mass of the atoms.

effective interaction strength can be changed in two ways [17]. One way is by changing the interaction strength g by using a Feshbach resonance, and another way is by changing the harmonic trap frequency [17].

For a dilute and weakly-interacting Bose gas, the ground-state energy is calculated within the Bogoliubov approximation [17]. In 1D, this gives

$$E_0 = \frac{N^2 g_{1\mathrm{D}}}{d} + \frac{1}{2}\sum_{p\neq 0}(\varepsilon(p) - p^2 - 2\rho^2\gamma), \tag{5.3}$$

where $\varepsilon(p) = |p|\sqrt{p^2 + 4\rho^2\gamma}$ is the elemental excitation spectrum, $\rho = N/L$ the number density of particles and $\gamma = g_{1\mathrm{D}}/(2\rho)$ [17]. One (or multiple) slabs will 'split' our condensate and the boundary condition used then is $\phi(0) = \phi(d) = 0$ where d is the distance between the two slabs [17]. The first term in the above equation is zero-temperature classical pressure due to the interactions which gives no contribution to the Casimir force [17].

The Casimir energy can be defined according to [17] as the difference between the Bogoliubov quasi-particle vacuum energy in an infinite condensate and a finite condensate (this definition cancels infinities). The Casimir energy is thus:

$$E_C = \sum_{n=1}^{\infty} f(n) - \int_0^{\infty} f(n)\mathrm{d}n + \frac{1}{2}f(0), \tag{5.4}$$

where the function $f(n)$ is defined as $\rho^2[(n\pi/\rho d)\sqrt{(n\pi/\rho d)^2 + 4\gamma} - (n\pi/\rho d)^2 - 2\gamma]$ [17]. This partially comes from the dispersion relation. For a more detailed calculation see [17]. Using the Euler-Maclaurin theorem, the Casimir energy is:

$$E_C = -\frac{\rho\pi\sqrt{\gamma}}{6}\left(\frac{1}{d} - \frac{1}{80 g_{1\mathrm{D}} d^3}\right), \tag{5.5}$$

where higher order terms $(d^{-4}, ...)$ are neglected [17]. The Casimir force is:

$$F_C = -\frac{\partial E_C}{\partial d} = -\frac{\rho\pi\sqrt{\gamma}}{6d^2} + \frac{\rho\pi\sqrt{\gamma}}{240 g_{1\mathrm{D}} d^3}, \tag{5.6}$$

which clearly differs with the Casimir force found in three dimensions [17]. The main contribution to the Casimir force comes from the d^{-2} term, while in the 3D case it comes from the d^{-4} [17].

5.2 The RuBECi setup

Experiments on BECs will be performed in a collaboration between QuantumGroup@UGent and TQC (Universiteit Antwerpen) using the RuBECi© system of ColdQuanta [85]. The isotope used is ^{87}Rb. Part of the system is displayed in Figure 5.1. It consists of 2 magneto-optical traps (MOTs) and a vacuum chamber containing the condensate, including an atomic chip. The condensate is trapped by the fields generated by the atomic chip, and is imaged optically.

Name	Symbol	Value
Scattering length	a	52.9 Å
Frequency of trap	ω	1 kHz
"Trap length"	L	50 μm
Number of atoms	N	50000 atoms
Mass of atoms	m	$1.443{\cdot}10^{-25}$kg

Table 5.1: The approximate parameters of the experimental system used for the calculations.

Of course, it is the integrated (over one direction) optical density that is measured. For the order of magnitude calculations performed in this Thesis, the number of atoms can be approximated to be 50000 atoms and the frequency of the harmonic trap in the tight direction is of the order of 1 kHz. All the parameters used in the calculations are depicted in Table 5.1.

5.3 Experimental feasibility

5.3.1 Single plate

The Casimir force can be related to a change in the density which can be measured by using an extra laser pulse (cf. detuning). The unit of force is defined to be $f_0 = \frac{\hbar \mathrm{kHz}}{\mu \mathrm{m}} = 1.055 \cdot 10^{-25}\mathrm{N}$. Including the $\hbar$'s and masses gives for the Casimir force:

$$F_C = \left(-\frac{\rho\pi\sqrt{\gamma}}{6d^2\sqrt{2m}} + \frac{\rho\pi\sqrt{\gamma}\hbar^2}{240 g_{1\mathrm{D}} d^3 (2m)^{3/2}} \right) \frac{\mu\mathrm{m}}{\mathrm{kHz}} f_0. \tag{5.7}$$

The Casimir force has been plotted as a function of the distance d in Figure 5.3. The force is of the order of the force unit f_0 (for plates separated with a distance of 1 micron). This corresponds with a density via $F = \mu n$, where μ, in this case, can be calculated using the Thomas-Fermi limit.

The Thomas-Fermi approximation is shortly discussed because the chemical potential needed for the calculations is approximated by this method. This is based on [1]. An isotropic harmonic potential trap with frequency ω is considered here. The Gross-Pitaevskii energy functional can be split up into three parts: the kinetic energy, the confinement energy, and the interaction energy term:

$$E_{kin} = \int \Psi^*(\mathbf{r}) \left(-\frac{\hbar^2}{2m}\nabla^2 \right) \Psi(\mathbf{r}) d\mathbf{r}, \tag{5.8}$$

$$E_{conf} = \int \Psi^*(\mathbf{r}) \left(\frac{m\omega^2 r^2}{2} \right) \Psi(\mathbf{r}) d\mathbf{r}, \tag{5.9}$$

$$E_{int} = \int \Psi^*(\mathbf{r}) \left(\frac{g}{2}|\Psi(\mathbf{r})|^2 \right) \Psi(\mathbf{r}) d\mathbf{r}. \tag{5.10}$$

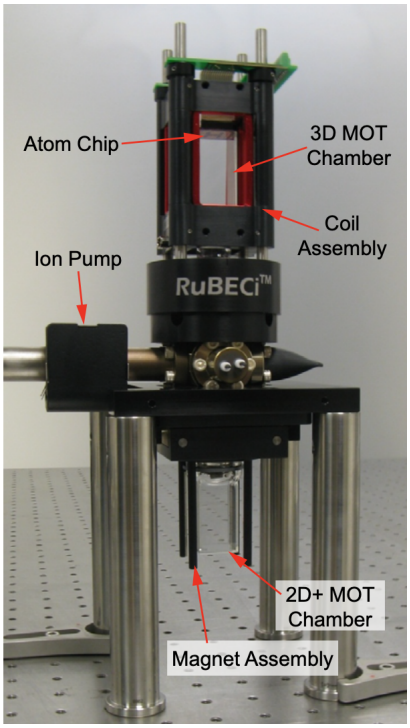

Figure 5.1: Part of the system described in [85]. It consists of 2 Magneto-Optical traps (MOTs) and a vacuum chamber containing the condensate of ^{87}Rb atoms of atoms, including an atomic chip. Source: [85]

The interaction energy can be approximated to be proportional to N/a_{HO}^2:

$$E_{int} \propto \frac{N}{a_{HO}^2}. \tag{5.11}$$

And thus, the ratio between interaction energy and kinetic energy becomes:

$$E_{int} \propto \frac{Na}{a_{HO}}, \tag{5.12}$$

which is called the *Thomas-Fermi parameter*. If the Thomas-Fermi parameter is much larger than 1 in absolute value, the kinetic energy is much smaller than the interaction energy and hence, it can be neglected. This is called the *Thomas-Fermi approximation*. This is frequently the case, this is why this will be assumed in the next section. Using this approximation, the Gross-Pitaevskii equation is solved straightforwardly:

$$n_{TF}(\mathbf{r}) = |\Psi(\mathbf{r})|^2 = \frac{m}{4\pi\hbar^2 a}(\mu - V_1(r)). \tag{5.13}$$

For a harmonic trap, this results in an inverted parabola density profile, as shown in Figure 5.2. The chemical potential can be found by making use of the

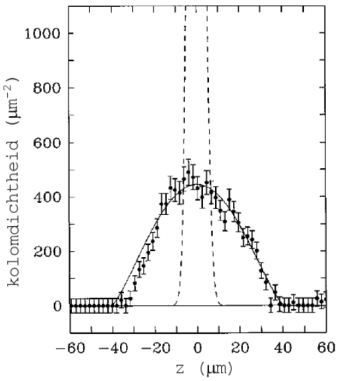

Figure 5.2: The density plotted as a function of distance to the center of the trap for a condensate consisting of 100000 atoms of ^{87}Rb. The experimental values can be nicely fitted by the Thomas-Fermi result (inverted parabola). Source: [1]

restriction on the number of atoms:

$$N = \int n_{TF}(\mathbf{r}) d\mathbf{r} \tag{5.14}$$

$$= \frac{m}{\hbar^2 a} \int_0^{\sqrt{2\mu/(m\omega^2)}} r^2(\mu - m\omega^2 r^2/2) dr, \tag{5.15}$$

$$\Rightarrow \mu = \frac{\hbar\omega}{2} \left(\frac{15Na}{a_{HO}} \right)^{2/5}. \tag{5.16}$$

In the Thomas-Fermi limit, the chemical potential is given by:

$$\mu = \frac{\hbar\omega}{2} \left(\frac{15Na}{a_\perp} \right)^{2/5}, \tag{5.17}$$

which only holds in three dimensions. Because an order of magnitude estimate is requested, the above formula is still a good estimate for the one-dimensional case. The one-dimensional case results in:

$$\mu = \frac{1}{2} \left(\frac{3}{2} N g_{1D} \sqrt{m\omega^2} \right)^{2/3}, \tag{5.18}$$

which results in a similar order of magnitude result. So, the above Casimir force corresponds with a change in density of a few atoms per micron. This could be measurable. The complete graph is shown in 5.3. It first is negative (and almost zero) but increases when the plates come very close.

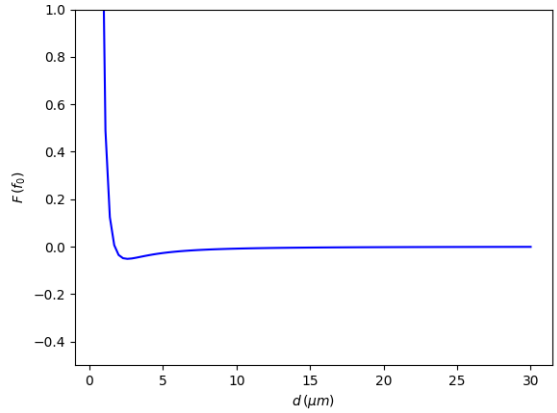

Figure 5.3: The Casimir force (in units of f_0) has been plotted as a function of the distance d (in units of microns).

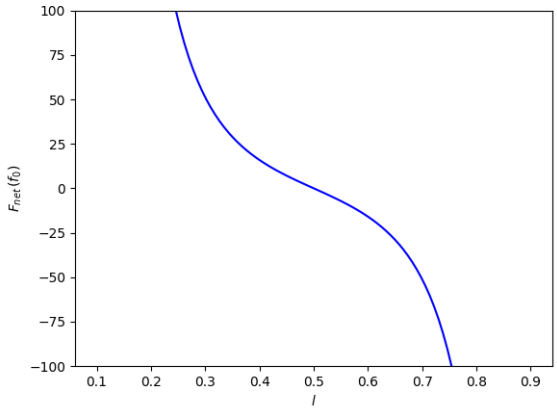

Figure 5.4: The Casimir force when an additional plate is introduced as a function of the fraction of the distance of the new plate. The total distance is set constant to 1 μm.

5.3.2 Multiple plates

In the case of one other plate in between the others, the force is the difference between the two forces on both parts of the system. When the additional plate is exactly in the middle, the two forces cancel and no net force is present. When the additional plate moves away from the middle, a net force is created. The net force as a function of the fraction of distance is shown in Figure 5.4 (where the total distance is set constant to 1 μm). Thus, the Casimir effect can possibly

be measured in the RuBECi setup, as can be concluded from the calculations. By varying the distance of a second plate, the Casimir force can be varied and may perhaps be better visible.

Chapter 6

Conclusion and Outlook

In this Thesis, we illustrated that Bose-Einstein condensates can be used as a platform to study quantum fluctuation effects that are inaccessible in other systems, including black holes. We have considered both the Casimir effect and Hawking radiation. The Casimir effect is the attraction of two parallel uncharged plates due to quantum vacuum fluctuations. Hawking proved that black holes are not "black" in quantum mechanics but emit radiation with a temperature of $T = \hbar g/(2\pi ck)$, which is called Hawking radiation.

The Casimir force was investigated for a quasi-one dimensional Bose-Einstein condensate using an effective Hamiltonian and the force obviously decreases as the plates are further away from each other. This can be applied to an experimental setup, e.g. the Cold Quanta setup that is currently being installed at the University of Ghent in collaboration with the UAntwerpen. By using order-of-magnitude estimations, we have found that the Casmimir force corresponds to a change in density of a few atoms per micron, which could be measurable.

The main topic in this thesis was the elaboration of the analogy between a Bose-Einstein condensate and a black hole by rewriting the hydrodynamic equations into a d'Alembertian with an effective acoustic metric, which is similar to the Schwarzschild one. Fluctuations of the phase field of the condensate, propagate in this curved geometry. This summarizes the idea of analogue gravity. The Bose-einstein condensate setup can be transformed into a sonic dumb hole by placing a sharp potential step at the origin $x = 0$, which acts as a horizon, with the speed of sound playing the role of the speed of light.

Signatures of Hawking radiation were found in numerical simulations performed within the Truncated Wigner Approximation (TWA), which includes quantum fluctuations by creating an ensemble of wavefunctions with initial quantum noise (using gaussian random numbers) and to propagate all of these using the GPE, where finally an average is taken. The interaction strength was made spatially-dependent to make side-effects, such as soliton shedding, minimal. This was the approach taken in [16]. In both cases, we have looked at the density-density correlation functions where several lines were visible. Fringes from the sudden modulation of the interaction strength were present (related

to the dynamical Casimir effect). Two lines were visible related to different Hawking modes. These results are in line with those in [16]. Also, we checked how to implement this experimentally and what the expected results would be using a change in transversal confinement. Other simulations apart from the step-sweep experiment were performed which includes the oscillating horizon experiment. In the case which includes a step-sweep, interference fringes can be observed in the spatial density autocorrelation function. Without a step-sweep, the Hawking radiation is merely visible. In the case of an oscillating horizon, excitations were visible when the speed of movement was made larger than the critical Landau velocity, to break superfluidity. Also, the case of a de Laval nozzle has been studied where the two horizons enhance the Hawking radiation and a checkerboard pattern is visible. Bragg spectroscopy was studied to measure the dispersions of the systems and look at stimulated Hawking radiation without quantum fluctuations. All of the simulations were performed with MATLAB.

A follow-up on this Thesis could be to experimentally observe the Casimir-Polder force and compare it to the results provided here and to look at other setups which may show Hawking radiation or even experimentally detect it in the RuBECi setup (it was already detected in other setups by Steinhauer in [22]). In addition, a deeper understanding or study of the excitations related to the oscillating horizon could be next. It would also be interesting to look at the "temperature" of the Hawking radiation, in detail.

Appendix A

MATLAB scripts

In this appendix, the general MATLAB script used for the numerical simulations is given. Some parameters may be different from one simulation to another.

```
% Start with initializing parameters
Temperature = 0.04;
hbar = 1;
m = 1;
as = 5.8*10^(-3);
dx = 0.5;
Lx = 256;
Nx = Lx/dx;
dt = 10^(-3);
dtobs = dt*10^3;
tmax = dtobs*200;
tobs = (0:dtobs:tmax);
g3D = 4*pi*hbar^2*as/m;
xx =(-Nx/2:Nx/2-1)'*dx;
kkx =(-Nx/2:Nx/2-1)'*2*pi/Lx;
mu0 = 0.5;
Uek=fftshift(exp(-1i*dt*(hbar^2*kkx.^2)/(2*m)));
Vx = zeros(Nx,tmax/dt);
Vxa = zeros(Nx,tmax/dt);
wp = 0.86*ones(Nx,tmax/dt);
h = mu0*0.75;
for it = 1:tmax/dt
    if it > tmax/(10*dt)
    v=-0.5*tanh((it-tmax/(10*dt)*1.1)/(tmax/(50*dt)));
    for x = 1:Nx
        if (v*it*dt<(x-Nx/2)*dx)
        Vx(x,it) = h;
```

```
28          Vxa(x,it) = h;
29          end
30      end
31      end
32      Vx(1,it) = h*100;
33      Vx(Nx,it) = h*100;
34      n_dens(it) = 50;
35      wp(:,it) = (0.5-Vxa(:,it))./(hbar*2*n_dens(it)*as)
            ;
36      g1D(:,it) = 2*hbar*as*wp(:,it);
37  end
38
39  % Ground state preparation using imaginary time
        evolution
40
41  mux=mu0-Vx(:,1);
42  mux(mux<0)=0;
43  psix=1*sqrt(mux./g1D(:,1));
44  psik=fft(psix);
45  Uim_ek=fftshift(exp(-dt*(hbar.^2*kkx.^2)/(2*m)));
46
47  taumax  = tmax;
48  for it=1:taumax/dt
49      psik=Uim_ek.*psik;
50      psix=ifft(psik);
51      psix=exp(-dt*(Vx(:,1)+g1D(:,1).*abs(psix).^2-mu0))
            .*psix;
52      psik=fft(psix);
53  end
54
55  psix_init = psix;
56  nxt_init = abs(psix_init).^2;
57
58  % Gross-Pitaevskii evolution
59  % This may include quantum fluctuations by using the
        Truncated Wigner Approximation (TWA)
60
61  xik=fftshift(hbar.^2*kkx.^2/(2*m));
62  epsk=sqrt(xik.*(2*mu0+xik));
63  uk=sqrt((xik+mu0)./(2*epsk)+0.5);
64  vk=-sqrt((xik+mu0)./(2*epsk)-0.5);
65
66  nreals=3000;
67  nxt=zeros(Nx,numel(tobs));
68  nn=zeros(Nx,Nx,numel(tobs));
69  nkt=zeros(Nx,numel(tobs));
```

```
70
71  for ireal=1:nreals
72      psix=psix_init;
73      Ak=1/2*1./(sqrt(tanh(fftshift(epsk)/(2*Temperature
            ))))).*(randn(Nx,1)+1i*randn(Nx,1));
74      Amkc=conj(Ak);
75      dpsi = zeros(Nx,1);
76      for i = 1:Nx
77          for pos = 1:Nx
78              if i ~= Nx/2+1
79                  ukn = fftshift(uk);
80                  vkn = fftshift(vk);
81                  dpsi(pos) = dpsi(pos)+...
82                      1/sqrt(Lx).*(Ak(i).*ukn(i).*exp(1i
                            .*kkx(i).*xx(pos))+...
83                      Amkc(i).*vkn(i).*exp(-1i.*kkx(i).*
                            xx(pos)));
84              end
85          end
86      end
87      psix = psix+dpsi;
88      psik=fft(psix);
89
90      psixt=zeros(Nx,numel(tobs));
91      psikt=psixt;
92      psixn = zeros(Nx,numel(tobs));
93      psikn = zeros(Nx,1);
94      nxt(:,1) = nxt_init;
95      t=0;
96      psixt(:,1)=psix;
97      psikt(:,1)=psik;
98      for it=1:tmax/dt
99          psik=Uek.*psik;
100         psix=ifft(psik);
101         psix=exp(-1i*dt*(Vx(:,it)+g1D(:,it).*abs(psix)
                .^2)).*psix;
102         psik=fft(psix);
103         t=t+dt;
104         if(any(abs(tobs-t)<0.1*dt)) % Store results
105             psixt(:,round(t/dtobs)+1)=psix;
106             psikt(:,round(t/dtobs)+1)=psik;
107             nxt(:,round(t/dtobs)+1)= nxt(:,round(t/
                    dtobs)+1)+...
108             abs(psix).^2/nreals;
109             nkt(:,round(t/dtobs)+1)= nkt(:,round(t/
                    dtobs)+1)+...
```

```
                fftshift(abs(psik).^2)/nreals;
            for k = 1:Nx
                for j = 1:Nx
                    nn(k,j,round(t/dtobs)+1) = nn(k,j,
                        round(t/dtobs)+1)+...
                        (abs(psix(k)).^2).*(abs(psix(j
                            )).^2)/nreals;
                end
            end
        end
    end
end

% Calculate density-density correlation function
G = zeros(Nx,Nx,201);
for t = 1:201
for k = 1:Nx
for j = 1:Nx
num = nn(k,j,t)+1/(4*dx^2)*(1+(j==k))-1/(2*dx)*(1+(j==
    k))*(nxt(j,t)+nxt(k,t));
denum1 = nxt(k,t)-1/(2*dx);
denum2 = nxt(j,t)-1/(2*dx);
G(j,k,t)=num./(denum1.*denum2)-1;
end
end
end

Gsmoothen = smoothdata(G,1,'gaussian',10);
Gsmoothen = smoothdata(Gsmoothen,2,'gaussian',10);
```

Bibliography

[1] J. Tempere. *Bose-Einstein Condensation, Superfluidity and Superconductivity*. 2020.

[2] Mike H Anderson et al. "Observation of Bose-Einstein condensation in a dilute atomic vapor". *Science* 269.5221 (1995), 198–201.

[3] Kendall B Davis et al. "Bose-Einstein condensation in a gas of sodium atoms". *Physical Review Letters* 75.22 (1995), 3969.

[4] Christopher Townsend, Wolfgang Ketterle, and Sandro Stringari. "Bose-Einstein condensation". *Physics World* 10.3 (1997), 29.

[5] *First Bose Einstein Condensate*. https://www.aps.org/publications/apsnews/200406/history.cfm. Accessed: 2021-12-31.

[6] Richard P Feynman. *Simulating physics with computers, International journal of theoretical physics*.

[7] Stephen W Hawking. "Black hole explosions?" *Nature* 248.5443 (1974), 30–31.

[8] Matt Visser. *Prof. Matt Visser - Analogue Hawking radiation?* Youtube. 2020. URL: https://www.youtube.com/watch?v=JJqWz7xCDsU.

[9] Carlos Barceló, Stefano Liberati, and Matt Visser. "Analogue gravity". *Living reviews in relativity* 14.1 (2011), 1–159.

[10] William G Unruh. "Notes on black-hole evaporation". *Physical Review D* 14.4 (1976), 870.

[11] *The Casimir Effect*. https://www.theo.phys.ulg.ac.be/~{c}ugnon/cas.pdf. Accessed: 2021-12-31.

[12] Francesco Intravaia. "Casimir Effect and Interaction between Surface Plasmons". PhD thesis. Université Pierre et Marie Curie-Paris VI, 2005.

[13] Christopher M Wilson et al. "Observation of the dynamical Casimir effect in a superconducting circuit". *Nature* 479.7373 (2011), 376–379.

[14] A Torode. "Exploration of the Quantum Casimir Effect". *Student Journal Of Physics* 6.2 (2017).

[15] Alexander Stange, David K Campbell, and David J Bishop. "Science and technology of the Casimir effect". *Physics Today* 74.1 (2021), 42–48.

[16] Iacopo Carusotto et al. "Numerical observation of Hawking radiation from acoustic black holes in atomic Bose–Einstein condensates". *New Journal of Physics* 10.10 (2008), 103001.

[17] Xiao-Lu Yu et al. "Casimir forces in a quasi–one-dimensional trapped dilute Bose gas". *EPL (Europhysics Letters)* 85.1 (2009), 10005.

[18] Iacopo Carusotto and Roberto Balbinot. "Acoustic Hawking radiation". *Nature Physics* 12.10 (2016), 897–898.

[19] Jeff Steinhauer. "Observation of self-amplifying Hawking radiation in an analogue black-hole laser". *Nature Physics* 10.11 (2014), 864–869.

[20] Yi-Hsieh Wang et al. "Mechanism of stimulated Hawking radiation in a laboratory Bose-Einstein condensate". *Physical Review A* 96.2 (2017), 023616.

[21] Jeff Steinhauer. "Measuring the entanglement of analogue Hawking radiation by the density-density correlation function". *Physical Review D* 92.2 (2015), 024043.

[22] Jeff Steinhauer. "Observation of quantum Hawking radiation and its entanglement in an analogue black hole". *Nature Physics* 12.10 (2016), 959–965.

[23] Juan Ramón Muñoz de Nova et al. "Observation of thermal Hawking radiation and its temperature in an analogue black hole". *Nature* 569.7758 (2019), 688–691.

[24] Shyamal Biswas et al. "Casimir force on an interacting Bose–Einstein condensate". *Journal of Physics B: Atomic, Molecular and Optical Physics* 43.8 (2010), 085305.

[25] Iacopo Carusotto et al. "Density correlations and analog dynamical Casimir emission of Bogoliubov phonons in modulated atomic Bose-Einstein condensates". *The European Physical Journal D* 56.3 (2010), 391–404.

[26] J-C Jaskula et al. "Acoustic analog to the dynamical Casimir effect in a Bose-Einstein condensate". *Physical Review Letters* 109.22 (2012), 220401.

[27] DM Harber et al. "Measurement of the Casimir-Polder force through center-of-mass oscillations of a Bose-Einstein condensate". *Physical Review A* 72.3 (2005), 033610.

[28] Albert Einstein. "Quantentheorie des einatomigen idealen Gases". *Albert Einstein: Akademie-Vorträge: Sitzungsberichte der Preußischen Akademie der Wissenschaften 1914–1932* (2005), 237–244.

[29] Cl C Bradley et al. "Evidence of Bose-Einstein condensation in an atomic gas with attractive interactions". *Physical review letters* 75.9 (1995), 1687.

[30] Eugene P Gross. "Structure of a quantized vortex in boson systems". *Il Nuovo Cimento (1955-1965)* 20.3 (1961), 454–477.

[31] Lev P Pitaevskii. "Vortex lines in an imperfect Bose gas". *Sov. Phys. JETP* 13.2 (1961), 451–454.

[32] CA Regal, Markus Greiner, and Deborah S Jin. "Observation of resonance condensation of fermionic atom pairs". *Physical review letters* 92.4 (2004), 040403.

[33] Lev Pitaevskii and Sandro Stringari. *Bose-Einstein condensation and superfluidity*. Volume 164. Oxford University Press, 2016.

[34] *Kinetic Temperature*. http://hyperphysics.phy-astr.gsu.edu/hbase/Kinetic/kintem.html. Accessed: 2021-12-31.

[35] Louis De Broglie. "Waves and quanta". *Nature* 112.2815 (1923), 540–540.

[36] Louis de Broglie. "XXXV. A tentative theory of light quanta". *The London, Edinburgh, and Dublin Philosophical Magazine and Journal of Science* 47.278 (1924), 446–458.

[37] Wolfgang Pauli. "Über den Zusammenhang des Abschlusses der Elektronengruppen im Atom mit der Komplexstruktur der Spektren". *Zeitschrift für Physik* 31.1 (1925), 765–783.

[38] Giovanni Lombardi. "Effective field theory for superfluid Fermi gases: application to polarons and solitons". PhD thesis. University of Antwerp, 2017.

[39] Nick Verhelst. *Over vortices en vortexstructuren in ultrakoude kwantumgassen*. University of Antwerp, 2019.

[40] William D Phillips and Harold J Metcalf. "Cooling and trapping atoms". *Scientific American* 256.3 (1987), 50–57.

[41] Claude N Cohen-Tannoudji and William D Phillips. "New mechanisms for laser cooling". *Phys. Today* 43.10 (1990), 33–40.

[42] Steven Chu. "Laser trapping of neutral particles". *Scientific American* 266.2 (1992), 70–77.

[43] CJ Myatt et al. "Production of two overlapping Bose-Einstein condensates by sympathetic cooling". *Physical Review Letters* 78.4 (1997), 586.

[44] *Lecture 6: Laser Cooling of Atoms*. https://web.stanford.edu/~{r}pam/dropoff/Phys041N/lecture6-lasercooling.pdf. Accessed: 2021-12-31.

[45] *Evaporative cooling*. https://sites.ualberta.ca/{223c}ljleblan/background/evaporative-cooling.html. Accessed: 2021-12-31.

[46] Cheng Chin et al. "Feshbach resonances in ultracold gases". *Reviews of Modern Physics* 82.2 (2010), 1225.

[47] Mathias Van Regemortel. "Quasiparticles in Out-of-equilibrium Quantum Systems: Correlations and Equilibration". PhD thesis. Universiteit Antwerpen, 2018.

[48] S Inouye et al. "Observation of Feshbach resonances in a Bose–Einstein condensate". *Nature* 392.6672 (1998), 151–154.

[49] Ph Courteille et al. "Observation of a Feshbach resonance in cold atom scattering". *Physical Review Letters* 81.1 (1998), 69.

[50] Selim Jochim et al. "Bose-Einstein condensation of molecules". *Science* 302.5653 (2003), 2101–2103.

[51] Luca Giacomelli. "Superradiant phenomena: Lessons from and for Bose–Einstein condensates". PhD thesis. Università di Trento, 2021.

[52] Hendrik BG Casimir and Dirk Polder. "The influence of retardation on the London-van der Waals forces". *Physical Review* 73.4 (1948), 360.

[53] Hendrick BG Casimir. "On the attraction between two perfectly conducting plates". *Proc. Kon. Ned. Akad. Wet.* Volume 51. 1948, 793.

[54] Steven K Lamoreaux. "Demonstration of the Casimir force in the 0.6 to 6 μ m range". *Physical Review Letters* 78.1 (1997), 5.

[55] Tao Gong et al. "Recent progress in engineering the Casimir effect–applications to nanophotonics, nanomechanics, and chemistry". *Nanophotonics* 10.1 (2021), 523–536.

[56] Umar Mohideen and Anushree Roy. "Precision measurement of the Casimir force from 0.1 to 0.9 μ m". *Physical Review Letters* 81.21 (1998), 4549.

[57] Trang T Nguyen. "Casimir effect and vacuum fluctuations". *Department of Physics and Astronomy, Ohio University* (2003).

[58] Kimball A Milton. *The Casimir effect: physical manifestations of zero-point energy*. World Scientific, 2001.

[59] Sixty Symbols and Prof. Mike Merrifield. *Casimir Effect Black Holes - Sixty Symbols*. Youtube. 2014. URL: https://www.youtube.com/watch?v=IRcmqZkGOK4.

[60] Shyamal Biswas, Saugata Bhattacharyya, and Amit Agarwal. "Casimir effect for a Bose–Einstein condensate inside a cylindrical tube". *Journal of Physics B: Atomic, Molecular and Optical Physics* 49.1 (2015), 015301.

[61] Nguyen Van Thu, Luong Thi Theu, and Dang Thanh Hai. "Casimir and Surface Tension Forces on a Single Interacting Bose–Einstein Condensate in Canonical Ensemble". *Journal of Experimental and Theoretical Physics* 130.3 (2020), 321–326.

[62] Sean M Carroll. *Spacetime and geometry*. Cambridge University Press, 2019.

[63] *Hawking-Unruh Radiation and Radiation of a Uniformly Accelerated Charge*. https://www.hep.princeton.edu/~{m}cdonald/accel/unruhrad.pdf. Accessed: 2021-12-31.

[64] Cesar A Uliana Lima et al. "Probing the Unruh effect with an accelerated extended system". *Nature communications* 10.1 (2019), 1–11.

[65] *Unruh Radiation*. https://www.research.kobe-u.ac.jp/fsci-pacos/SeminarFiles/2016yamamoto.pdf. Accessed: 2021-12-31.

[66] *The Unruh effect: interpretation and applications to neutrino physics*. https://indico.cern.ch/event/322559/contributions/748503/attachments/623891/858522/giorgio_torrieri.pdf. Accessed: 2021-12-31.

[67] Jiazhong Hu et al. "Quantum simulation of Unruh radiation". *Nature Physics* 15.8 (2019), 785–789.

[68] Roberto Balbinot et al. "Nonlocal density correlations as a signature of Hawking radiation from acoustic black holes". *Physical Review A* 78.2 (2008), 021603.

[69] Francesco Belgiorno et al. "Hawking radiation from ultrashort laser pulse filaments". *Physical review letters* 105.20 (2010), 203901.

[70] E Rubino et al. "Experimental evidence of analogue Hawking radiation from ultrashort laser pulse filaments". *New Journal of Physics* 13.8 (2011), 085005.

[71] Silke Weinfurtner et al. "Measurement of stimulated Hawking emission in an analogue system". *Physical review letters* 106.2 (2011), 021302.

[72] Eugene P Wigner. "On the quantum correction for thermodynamic equilibrium". *Part I: Physical Chemistry. Part II: Solid State Physics*. Springer, 1997, 110–120.

[73] Alice Sinatra, Carlos Lobo, and Yvan Castin. "The truncated Wigner method for Bose-condensed gases: limits of validity and applications1". *Journal of Physics B: Atomic, Molecular and Optical Physics* 35.17 (2002), 3599.

[74] MJ Steel et al. "Dynamical quantum noise in trapped Bose-Einstein condensates". *Physical Review A* 58.6 (1998), 4824.

[75] Carlo F Barenghi and Nick G Parker. *A primer on quantum fluids*. Springer, 2016.

[76] Jonathan Wurtz, Anatoli Polkovnikov, and Dries Sels. "Cluster truncated Wigner approximation in strongly interacting systems". *Annals of Physics* 395 (2018), 341–365.

[77] Russell P Rundle and Mark J Everitt. "Overview of the phase space formulation of quantum mechanics with application to quantum technologies". *Advanced Quantum Technologies* (2021), 2100016.

[78] P Blair Blakie et al. "Dynamics and statistical mechanics of ultra-cold Bose gases using c-field techniques". *Advances in Physics* 57.5 (2008), 363–455.

[79] M Yuhao Liu, M Alberto Bramati, and M Maxime Jacquet. "Simulation of a 1D black hole in a superfluid of polaritons" (2020).

[80] A Recati, N Pavloff, and Iacopo Carusotto. "Bogoliubov theory of acoustic Hawking radiation in Bose-Einstein condensates". *Physical Review A* 80.4 (2009), 043603.

[81] Victor I Kolobov et al. "Observation of stationary spontaneous Hawking radiation and the time evolution of an analogue black hole". *Nature Physics* 17.3 (2021), 362–367.

[82] Carlos Barceló, Stefano Liberati, and Matt Visser. "Towards the observation of Hawking radiation in Bose–Einstein condensates". *International Journal of Modern Physics A* 18.21 (2003), 3735–3745.

[83] J Stenger et al. "Bragg spectroscopy of a Bose-Einstein condensate". *Physical Review Letters* 82.23 (1999), 4569.

[84] Carlos Mayoral et al. "Acoustic white holes in flowing atomic Bose–Einstein condensates". *New Journal of Physics* 13.2 (2011), 025007.

[85] Daniel M Farkas, Evan A Salim, and Jaime Ramirez-Serrano. "Production of Rubidium Bose-Einstein condensates at a 1 Hz rate". *arXiv preprint arXiv:1403.4641* (2014).